Magnetic Properties of a Bermudian Pillowed Lava Flow

by

George M. Dineen

Submitted in partial fulfillment of the requirements for the degree of Bachelor of Science with Honours in Geology, Dalhousie University, Halifax, Nova Scotia.

January 1982

Distribution License

DalSpace requires agreement to this non-exclusive distribution license before your item can appear on DalSpace.

NON-EXCLUSIVE DISTRIBUTION LICENSE

You (the author(s) or copyright owner) grant to Dalhousie University the non-exclusive right to reproduce and distribute your submission worldwide in any medium.

You agree that Dalhousie University may, without changing the content, reformat the submission for the purpose of preservation.

You also agree that Dalhousie University may keep more than one copy of this submission for purposes of security, back-up and preservation.

You agree that the submission is your original work, and that you have the right to grant the rights contained in this license. You also agree that your submission does not, to the best of your knowledge, infringe upon anyone's copyright.

If the submission contains material for which you do not hold copyright, you agree that you have obtained the unrestricted permission of the copyright owner to grant Dalhousie University the rights required by this license, and that such third-party owned material is clearly identified and acknowledged within the text or content of the submission.

If the submission is based upon work that has been sponsored or supported by an agency or organization other than Dalhousie University, you assert that you have fulfilled any right of review or other obligations required by such contract or agreement.

Dalhousie University will clearly identify your name(s) as the author(s) or owner(s) of the submission, and will not make any alteration to the content of the files that you have submitted.

If you have questions regarding this license please contact the repository manager at dalspace@dal.ca.

Grant the distribution license by signing and dating below.

_____ _____

Name of signatory Date

TABLE OF CONTENTS

TABLE OF CONTENTS (Continued)

LIST OF FIGURES

LIST OF TABLES

ABBREVIATIONS AND SYMBOLS

°C	Degrees Celsius
cm	centimeter
DIRM	Drilling Induced Remanent Magnetization
DSDP	Deep Sea Drilling Project
emu	electro magnetic unit
J	Magnetic intensity
Jo	Magnetic intensity at 0 Oe demagnetizing field
J200	Magnetic intensity at 200 Oe demagnetizing field
Jstable	Magnetic intensity at the stable inclination
km	kilometer
m	meter
mm	millimeter
u	10^{-6} m = 1 micrometer
Ma	10^{6} years
MDF	Mean Demagnetizing Field
NRM	Natural Remanent Magnetism
Oe	Oersted
TRM	Thermal Remanent Magnetism

ABSTRACT

This study is concerned with the description and interpretation of the opaque mineralogy and paleomagnetic properties of a 3.0 m core interval which is comprised of a pillowed lava flow and basal intrusive sheet taken from a depth of 776 m in an 802 m core drilled on the Bermuda Seamount. Results indicate that the observed magnetic properties are controlled by inter-related and generally non-separable effects of grain size, magnetic phase volume and alteration. Secondary mineralization and inclination polarity within the flow unit indicate that the flow has been magneticly overprinted by a normal polarity magnetic event and hydrothermal alteration associated with mid-Tertiary sheet intrusion. The remanence of the sheet and flow is of low intensity and is primarily carried by secondary magnetite formed at sub-Curie point temperatures. Original Cretaceous reverse magnetization of the flows is not separable from the normal polarity of the sheet since both magnetic components are likely to be carried by nearly pure magnetite of similar grain size. Shallow reverse and steep normal inclinations are interpreted as the resultant magnetic vectors of a frequently reversing geomagnetic field and a secondary shallow chemical remanent magnetization.

The flow and sheet units are characterized by type 2 and type 1 titanomagnetite, respectively. The opaque phases display extensive alteration ranging from grain cracking to complete granulation and numerous styles of titanohematite replacement.

High temperature and tectonic adjustment within the lava sequence at the depth of the core interval may contribute to the high degree of alteration and dipolar inclination dispersion observed.

I INTRODUCTION: THE BERMUDA SEAMOUNT

1.1 Seamounts and Previous Bermuda Results

The Bermuda Islands, located one-third of the distance from Cape Hatteras to the Mid-Atlantic Ridge, occupy the southeastern 7 percent of the 116 square kilometer Bermuda Seamount pedestal which rises 6000 m above the surrounding ocean floor and is the most northern, largest and only emergent one of three seamounts on the Bermuda Rise. Seamounts, defined as isolated volcanic edifices rising at least 1000 m from the ocean floor are features common to all oceanic basins. Some occur as chains or provinces that may include emergent tholeiitic to alkali basalt islands. Dredged material from the rise flanks has been the primary source of material for studies of seamount geology. This, however, may introduce a sampling bias to the experimental conclusions. Drilling is the preferred method for obtaining meaningful lithological and stratigraphic information.

Drilling in Bermuda in 1912 and 1958 established the presence of volcanic rocks beneath a sedimentary sequence that is overlain by subaerial limestone. Seismic reflection profiles across Castle Harbour (Figure 1) indicate that, in this area, the average interface depth between sediments and the seamount's volcanic sequence is 43 m below sea level (Gees and Medioli, 1970).

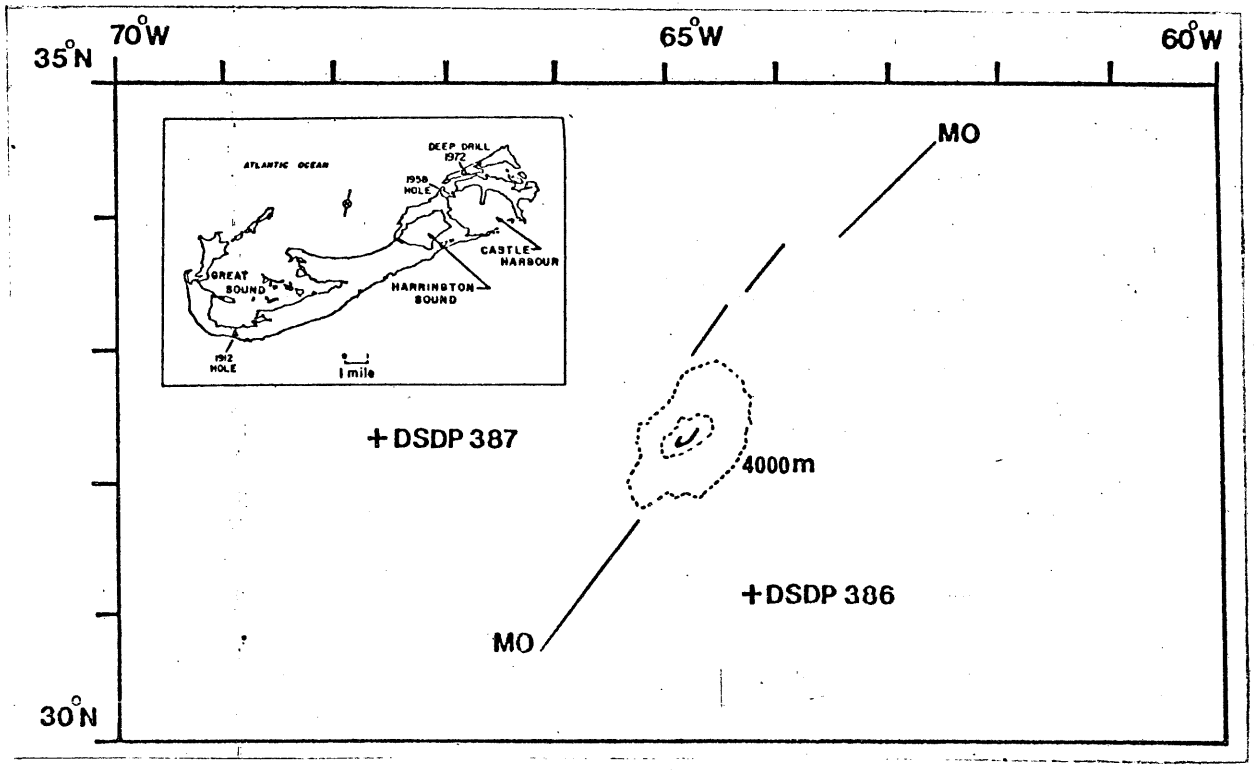

Figure 1. Bermuda Islands showing location of drill holes. The material described in this thesis was obtained from the Deep Drill 1972 hole. After Rice et al. (1980).

1.2 1972 Drilling in Bermuda

In 1972 Dalhousie University participated in the drilling of an 802 m deep continuously cored hole into the Bermuda Seamount. This drill hole was located within the property of the Bermuda Biological Station at 32° 22'N, 64° 42'W. Drill core recovery was approximately 100% and maximum deviation from vertical was ±1°. The upper 35.4 m of the core consists of Pleistocene carbonates, red beds and volcanic soil (Schenk 1973). The remaining 767 m is comprised of 927 volcanic cooling units: 431 submarine pillows or flows of hydrothermally altered tholeiitic composition, 493 interleaved intrusive limburgitic sheets and 3 breccia units (Aumento and Ade-Hall 1973).

Aumento and Gunn (1974) observed that average flow thickness is 0.9 m, and average sheet thickness is 0.6 m. The lava flows are recognized as submarine pillows or thin, rapidly cooled flows. A small proportion of the lavas are vesicular with calcite, zeolites, analcite and clay minerals. The original groundmass is vitreous to fine grained and consists of felted chlorite, calcite, analcite and clay minerals. The intrusive sheets are variably aphanitic to fine grained and some have phenocrysts of clinopyroxene, plagioclase, calcitic olivine pseudomorphs and magnetite as well as amygdaloidal cavities filled by calcite, zeolites, and quartz.

1.3 Age and Formation of the Bermuda Seamount

The Bermuda Rise obscures the position of magnetic anomaly Mo, lying just to the west and dated at 108-109 Ma by Larson and Hilde (1975). Consequently,

Bermuda may be as much as 5 Ma younger than anomaly Mo. Rice et al. (1980) suggest that if Bermuda formed simultaneously with the surrounding sea floor, its age would be 103 to 104 Ma. A minimum age of 91 $\pm$ 5 Ma for the flow unit and 33 Ma for the sheet intrusive event is suggested by K-Ar dates given by Reynolds and Aumento (1974).

Late Eocene (40 Ma) to Middle Oligocene (30 Ma) volcanogenic turbidites recovered at Deep Sea Drilling Project (DSDP) site 386 are consistent with the intrusive radiometric age, while basement ages as old as Albanian (103 Ma) and Valanginian (127 Ma) from DSDP sites 386 and 387, respectively, confirm the regional magnetic anomaly pattern (Tucholke et al. 1975); (see Figure 1). Geochemical data supports the two-stage formation process for Bermuda suggested by the K-Ar dates. The pillow flows are altered mid-ocean ridge basalts (Aumento et al. 1976) while the sheets are evolved limburgites with 5% $T;O_2$, 2% K_2O, 900 ppm sr and 500 ppm Ba at 40% $S;O_2$ (Aumento et al. 1975).

Extensive alteration has affected both flows and intrusives. Chloritization of glassy pillow margins and chlorite and hematite replacement is prevalent in the flow interiors. Aumento et al. (1976) conclude, through examination of secondary mineralization, that following halmyrolytic chemical alteration by ambient seawater at close to 2°C, the flows have been hydrothermally altered at temperatures in the range of 100°C to 200°C.

1.4 This Study

Submarine lava flows and pillowed basalts are the basic sea floor magnetic units. This study of the Bermuda core is concerned with the description and interpretation of several magnetic parameters and magnetic phase mineralogy through a 3.0 core interval that is comprised of an upper pillowed flow unit and an 80 cm basal sheet.

Paleomagnetic properties measured in this study include stable inclination, natural remanent magnetization (NRM) intensity at several alternating demagnetization field intensities, mean demagnetization field intensities and magnetic susceptibility. Opaque mineralogy descriptions are related, where possible, to the observed magnetic properties. A macroscopic description of the core is supplemented by a petrographic summary and thin-section descriptions.

Previous study of the Bermuda core by Rice (1977) has shown that hydrothermal alteration, associated with the sheet intrusion event, has overprinted the mid-Tertiary magnetization of the sheets onto the original Cretaceous reverse magnetization of the flows. The interpretations and conclusions in this study have been made in view of the previous Bermuda core results of Rice (1977) and Rice et al. (1980).

II CORE DESCRIPTION

1. Sampling and Sample Preparation

Samples were taken from minicores oriented perpendicular to the main core. Minicore position and frequency, given in Table 1 and Figure 2, allowed examination of core characteristics within and between flow and breccia units. Fiducial lines indicating true vertical were transferred from the main core to each minicore. The oriented minicores were cut approximately 2.0 to 2.5 cm in length so that they would fit in the digital spinner magnetometer sample holder. Thin sections and polished sections were made from the removed ends of the minicores. Polished and thin section numbers correspond to their respective minicore numbers.

2. Lithological Units

The core interval studied, taken from the 776.33 m to 779.37 m depth interval and defined as unit lava (UL) 131, is schematically shown in Figure 2. A full graphic summary and description of the core interval is given in Appendix 1.

The upper 2.1 m of the core consists of highly brecciated and altered black-green, calcitic debris with interbreccia zones of light grey, fine-grained, slightly amygdaloidal basalt. Minor calcitic breccia and chloritized inclusions occur in the interbreccia zones. The

TABLE 1. MINICORE SAMPLE POSITIONS

MINICORE SAMPLE NUMBER	DISTANCE OF SAMPLE ALONG CORE cm
1	1.5
4	18.0
5	23.0
6	27.7
7	37.5
8	45.0
9	66.5
10	72.5
11	110.5
12	133.0
13	150.3
14	167.0
15	173.5
16	180.5
17	196.0
18	212.0
21	237.3
22	248.0
23	253.5
24	261.5
25	276.3
26	284.0
27	294.7
28	268.5
29	288.6
32	202.3
34	128.7

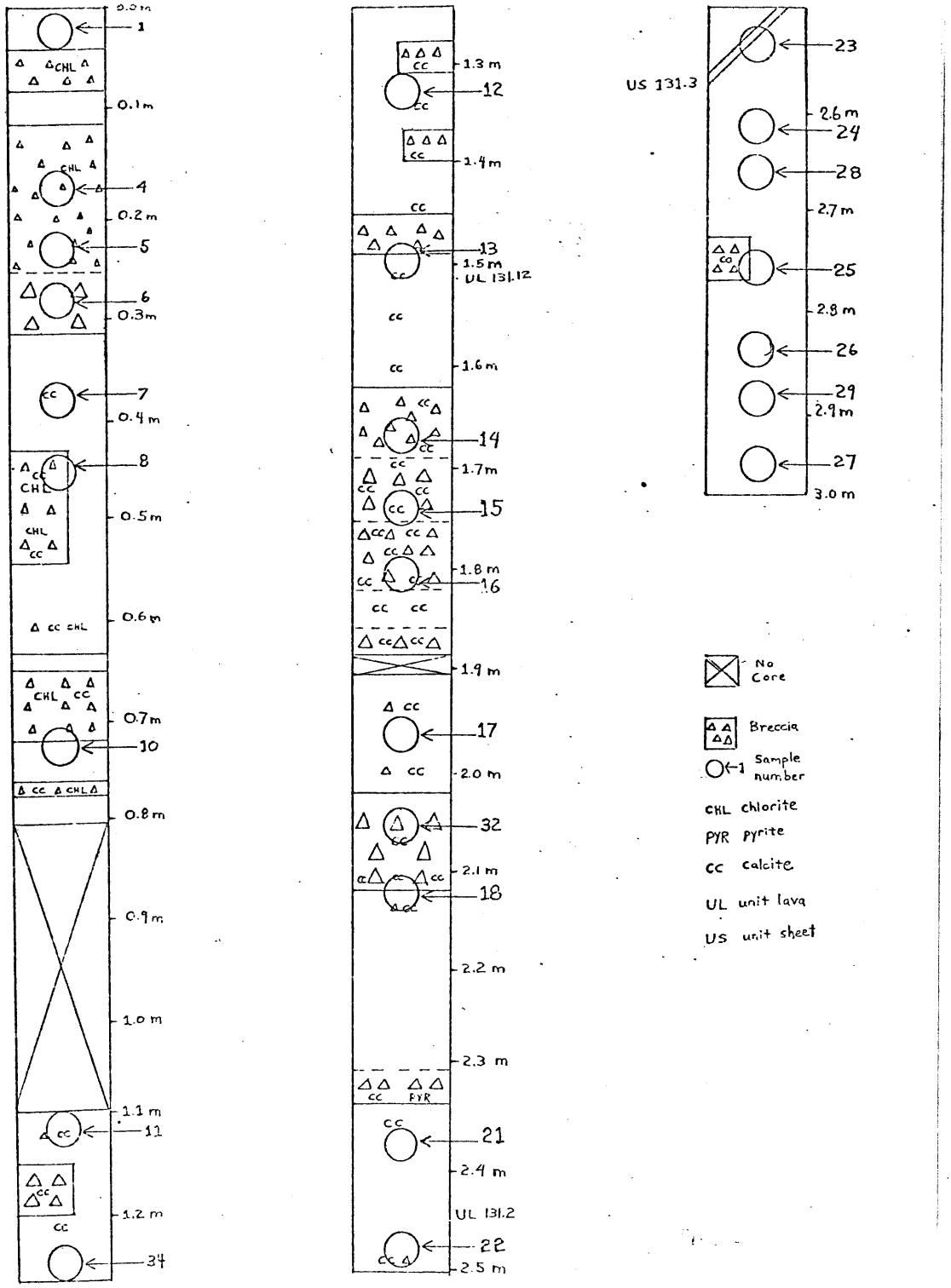

Figure 2. Schematic Core Diagram

lower 0.8 m of the core interval consists of predominantly fine to medium grained basalt. This division in core lithology was interpreted as representing an upper pillowed flow unit with pillow separation by thin lava flows and a massive basal sheet unit with minor breccia inclusions and chloritized calcitic zones. Breccia and calcite filled fractures in the basal sheet may be related to multiple lava flow intrusion or a non-uniform cooling history through the flow that produced localized chilled margins.

III PETROGRAPHIC SUMMARY

The upper 2.1 m of the core section consists of 11 highly brecciated and altered zones, interpreted as pillowed lava flow margins, which vary in thickness from 2 cm to 30 cm. These zones are separated by grey to dark grey, fine to medium grained, non-porphyritic, variolitic basalt. The basal 0.9 m of the core is primarily a non-porphyritic holocrystalline, calcite-clinopyroxene basalt sheet having minor alteration in comparison to the pillowed flow. Two minor breccia zones less than 5 cm in thickness and a 2 cm dike occur within the sheet.

Textural and structural style distinguishes the extrusive pillowed margins from the sheet unit at the core's base. The extrusive unit margins are highly brecciated and altered, particularly with chlorite which is pervasive throughout the brecciated margins and along calcite filled veins and fractures. Breccia clasts, interpreted as fragments of the cooling unit margins, are generally angular and variable in size up to 1.5 cm and bound in a mixed chloritic and carbonaceous cement.

Typically, the pillowed basalt margin has a chloritized exterior breccia zone enriched in mafic material that grades inward to a dark and mafic microporphyritic material. Chilled margins display a vitreous exterior that grades to a dark grey, crystalline material.

In thin section, the margins of the cooling units are spherulitic to cryptocrystalline with a high vitreous component. The groundmass is commonly vitrophyric and isotropic. In most cases, this matrix material is light brown, devitrified glass and has a pale green tint where chloritized. The brecciated cooling unit margins have vitrophyric breccia inclusions of spherulitic and microlitic plagioclase (30%). Up to 30% of the mineral assemblage may consist of calcite, primarily in veins and fractures. Opaque microphenocrysts (10%) are disseminated throughout the matrix and localized adjacent to breccia margins and calcite filled fractures.

Toward the center of the lava flow texture ranges from merocrystalline to hyalopilitic and intersertal. In general, the volume of plagioclase microphenocrysts and plagioclase grainsize increases away from the margins. Subhedral plagioclase (1.5 mm, 30% to 40%), calcite (30%) and opaque phases (5% to 10%) are the major minerals in a vitreous matrix. Intensity of chloritization over two 28 cm thick breccia units in the core interval shows a weak trend toward decreasing alteration with depth.

The basal sheet unit in the core section consists primarily of fine to medium grained, non-porphyritic, holocrystalline basalt. The upper 30 cm of this unit has an upper and lower breccia contact. In thin section basalt taken from the upper basalt, breccia contact is highly chloritized and hyalopilitic with intersertal plagioclase (1 mm) and few 1.5 mm plagioclase phenocrysts. Vesicles and amygdales are filled with quartz, tridymite and chlorite. Opaque minerals, estimated to compose 10% of the volume, are obscure dots and euhedral grains in the highly chloritized groundmass.

Forty-eight cm of fine to medium grained basalt lie beneath the lower breccia contact. This basalt is intruded by a single 2 cm wide dike 15 cm from its upper contact and is partially cut by a chloritized breccia unit 25 cm from its base. There is a rapid textural gradation in the basalt from spherulitic with minor pilotaxitic plagioclase in a variolitic matrix at the top of the unit to a granular holocrystalline assemblage of clinopyroxene (45%) intersertal with subhedral to euhedral plagioclase (1 mm, 35% to 40%). Minor calcite, (3% to 5%) occurs and very fine-grained opaque minerals (10%) are disseminated throughout the groundmass. Minor chloritization occurs, primarily around calcite filled fractures and vesicles. Basalt from the brecciated zone has an aphyric anhedral to subhedral granular texture composed of calcite olivine pseudomorphs, 10% to 15%; clinopyroxene, 30%; and plagioclase, 40%. The occurrence of considerable chlorite in fractures and as olivine pseudomorphs and spherulitic to microlitic plagioclase inclusions is distinctive.

An increase in grainsize and decrease in chloritization intensity is seen over the basal 25 cm of the core. Intersertal clinopyroxene (1.0 to 1.5 mm) is present in a groundmass containing calcite filled fractures and chlorite. Intersertal to microlitic plagioclase in a variolitic matrix occurs at the base of the core section. Anhedral to subhedral clinopyroxene is finer grained and chloritization is more disseminated than in the overlying flow unit.

IV ROCK MAGNETISM AND PILLOW LAVA

1. Controls of Natural Remanence Intensity

The natural remanent magnetization (NRM) intensity of a rock depends on the concentration of titanomagnetite, its composition and average grain size. Titanomagnetite grainsize is normally more important in the control of magnetic properties of basalt than the titanomagnetite volume (Ryall and Ade-Hall 1975, Smith and Prévot, 1977).

Dunlop (1973) states that very small titanomagnetite grains (<1 u) make the dominant contribution to NRM intensity because of a high remanence to unit volume ratio. The NRM intensity (emu/cm^3) of a magnetic grain is proportional to d^{-1}, and since grain volume is proportional to d^3, NRM intensity of the grain is proportional to d^2. This suggests that if very small grains are to be the primary carriers of magnetic remanence, then there must be many more of them than there are of larger grains.

The dependence of NRM intensity on grain diameter is shown in Figure 3. Two restrictions qualify the application of this relationship to natural skeletal titanomagnetite. The relationship is largely based on the results of Parry (1965) which were obtained using synthetic magnetite. Secondly, at very small grain size, single domain magnetic behavior does not persist, so NRM decreases.

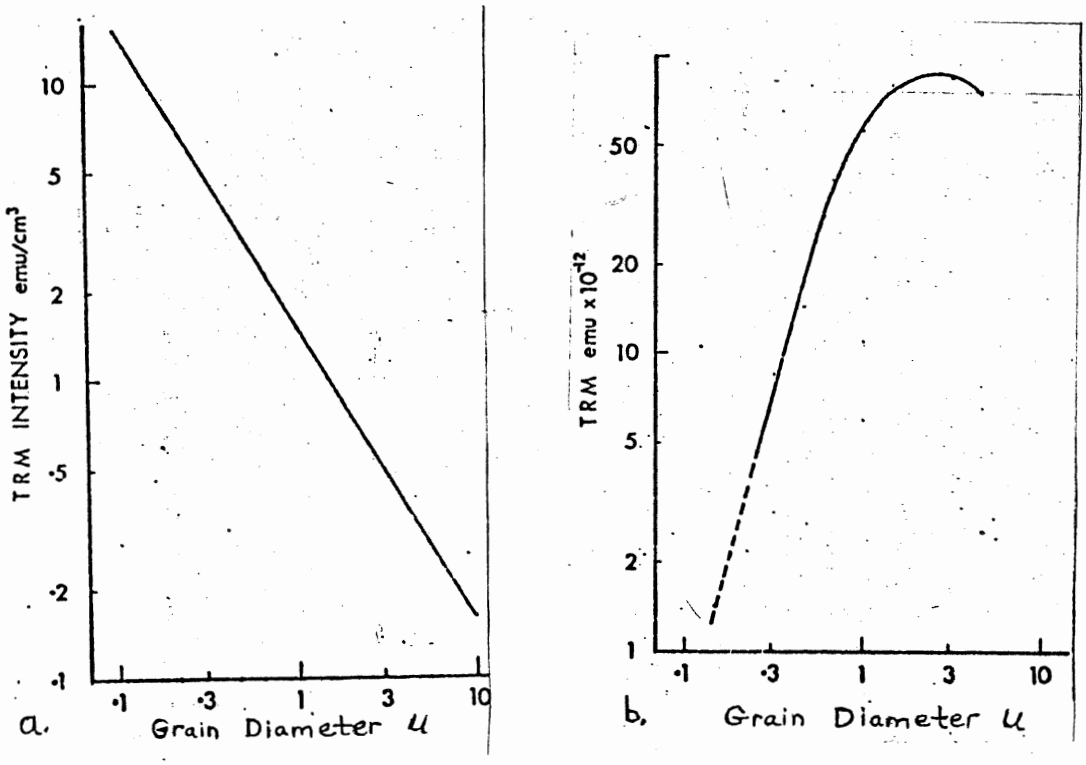

Figure 3. Relation between TRM and grain size

a) Intensity of TRM (emu/cm^3) as a function of grain diameter. Dunlop (1973) Fig. 7

b) Intensity of TRM as a function of grain size calculated for an area examined by Evans and Wayman. Grains of a few microns dominate TRM. The integral of the curve is the total TRM TRM of the sample.

2. Magnetic Characteristics of Pillow Basalt

The pillow flow is the basic sea floor magnetic unit. The major magnetic parameters of the pillow basalt are controlled by the percentage of titanomagnetite present, its grainsize, volume, and the degree of alteration. Grain size and extent of deuteric alteration are functions of the cooling history of the magma. Hydrothermal alteration is a function of the exposure of the submarine basalt to heated seawater at 10's degrees Celsius to several 100's degrees Celsius.

The flow of oxygenated water along interpillow contact zones and fractures during low temperature hydrothermal alteration results in varying degrees of titanomagnetite grain cracking, titanomaghemite replacement and granulation alteration. The circulation of ambient bottom seawater at or near 2° Celsius through the pillowed lava flow results in chemical halmyrolytic alteration. Marshall and Cox (1972) have determined that titanomagnetite alteration and sea floor weathering of pillow basalt results in a 40% reduction in NRM intensity and saturation magnetization values.

In submarine pillow basalts, Curie temperature typically increases toward the chilled pillow margin while NRM, saturation magnetization and magnetic susceptibility increase toward the pillow center (Marshall and Cox, 1972; Ryall and Ade-Hall, 1975). Marshall and Cox (1972) observed that the NRM intensity maximum for a single pillow lies within 2 cm of the pillow exterior. This magnetic intensity peak is a result of the cooling history of the pillow which is controlled by pillow

radius. They conclude that the intensity of remanence in igneous bodies with chilled margins attains a maximum level where crystallization is nearly complete. The NRM maximum will decline from the outer margin toward the pillow center as grain size of the magnetic phase becomes larger.

The most effective carriers of NRM in pillow basalt primarily due to their abundance, are skeletal titanomagnetite grains about 5 u across (Ryall and Ade-Hall, 1975). Grains of less than 3 u will be single or pseudosingle, and in general, the most magneticly significant range of grain sizes is between 0.5 u and 5.0 u (Rice 1977). Enhanced remanence at the pillow margin is primarily the result of more complete crystallization as well as secondary enrichment of magnetic phases giving greater titanomagnetite volume. Alteration processes have reduced the range of titanomagnetite grainsize. Rice (1977) observed that high saturation magnetization values at chilled flow contact margins reflects a high volume of titanomagnetite; a large percentage of which may be submicroscopic in the highly altered matrix.

V NATURAL REMANENCE INTENSITY

1. Equipment

A Schonstedt DSM-1 digital spinner magnetometer measured sample magnetization over an alternating field demagnetization scheme that used the following peak intensities: 0.0 to 100 Oersteds (Oe) in 25 Oe increments, 100 to 400 Oe in 50 Oe increments, 400 to 600 Oe in 100 Oe increments, and finally, 600 to 800 Oe in 200 Oe increments.

2. Results: J stable

Stable natural remanent magnetic moments of the samples range from 4.8×10^{-6}emu/cc to 4.5×10^{-3}emu/cc (Table 2).

The plot of log J stable versus inclination modulus (Figure 4) shows 3 disperse groups of points. Two groups have inclination modulii between 65° and 80° and have either high J stable values; greater than 8×10^{-4}emu/cc or low J stable values; less than 9×10^{-6}emu/cc. The third, largest and most disperse point group has inclination modulii between 46° and 85° and log J stable values intermediate between the other two-point groups; 4.0×10^{-5}emu/cm^3 to 4.0×10^{-4}emu/cm^3.

TABLE 2. SAMPLE INCLINATION, J STABLE AND J 200 VALUES

Sample Number	Inclination	J stable emu/cm^3	J 200 emu/cm^3
3	-64.3	6.46×10^{-5}	6.16×10^{-5}
6	-45.9	2.70×10^{-4}	3.58×10^{-4}
7	-70.2	2.50×10^{-4}	6.96×10^{-4}
10	+52.7	1.76×10^{-4}	5.62×10^{-5}
11	+82.9	6.03×10^{-4}	4.06×10^{-4}
12	+85.2	3.47×10^{-4}	3.47×10^{-4}
13	-66.2	1.55×10^{-3}	7.96×10^{-4}
15	-47.8	5.13×10^{-5}	7.78×10^{-4}
17	+72.7	1.25×10^{-3}	4.61×10^{-5}
18	+61.2	5.44×10^{-5}	5.44×10^{-5}
21	+57.3	5.56×10^{-5}	2.53×10^{-4}
22	-77.5	1.56×10^{-3}	5.63×10^{-4}
26	+67.3	7.32×10^{-6}	1.13×10^{-5}
28	+77.1	1.47×10^{-3}	3.37×10^{-5}
29	-72.0	1.44×10^{-3}	2.02×10^{-5}
32	+71.0	3.26×10^{-4}	5.21×10^{-5}

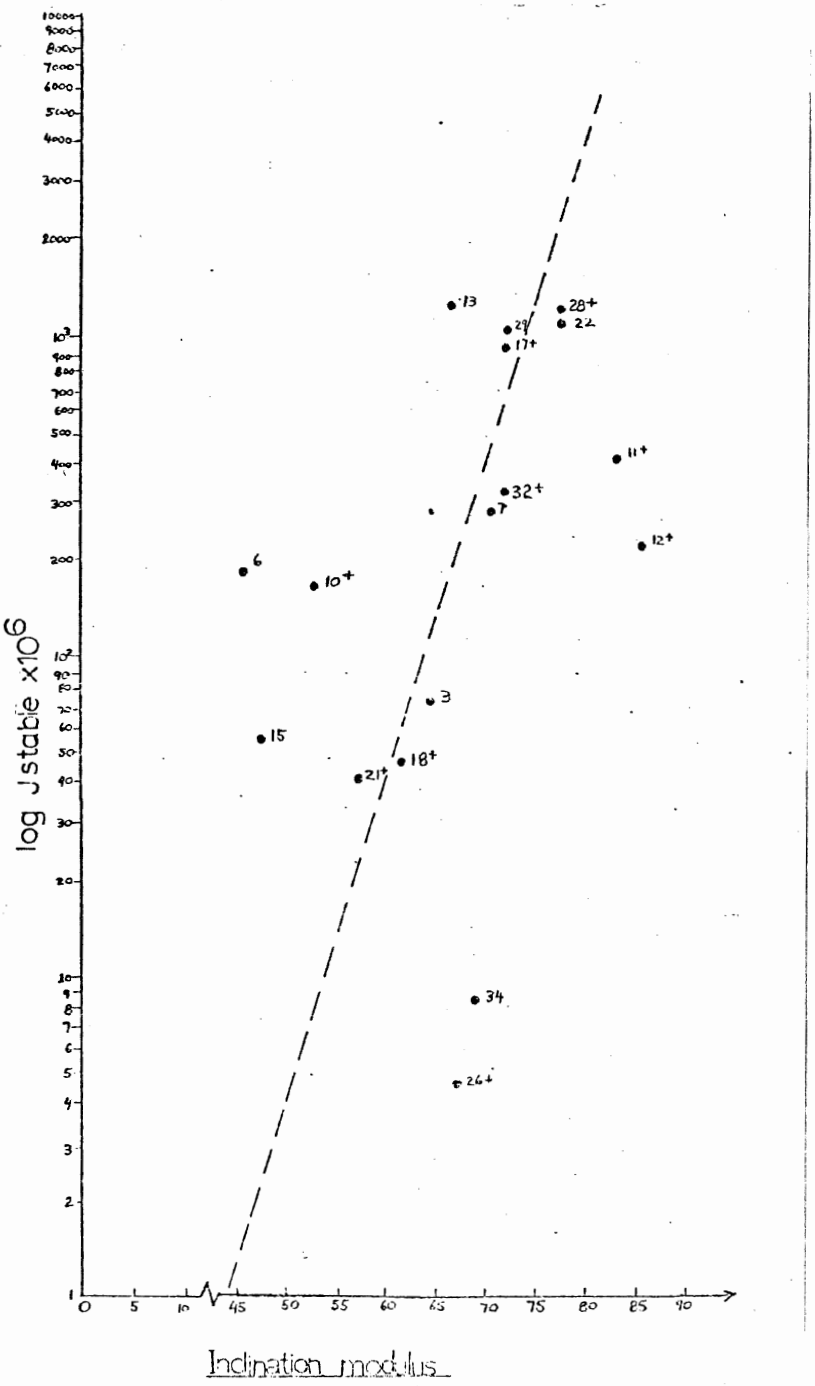

Figure 4. Plot of log J stable x 10^6 versus Inclination Modulus. Broken line is a linear regression line for the data.

There is no direct relationship between NRM intensity and lithological characteristics, degree of alteration or tectonic modification in the core. In thin section, the small grainsize and dispersion of the titanomagnetites, the superposition of two or more generations of titanomagnetite grainsize, alteration and secondary mineralization at unit margins prevents correlation of NRM and MDF profiles with the core's lithological zones.

3. Results: J stable and J 200

3.1 Flow and Sheet NRM

A contrast in NRM intensity between the basal sheet and the pillowed flow is indicated by comparison of average J 200 and J stable values from these units. The sheet has a J 200 value of $1.55 \times 10^{-4} emu/cm^3$ and the J 200 value of the flow unit is $3.50 \times 10^{-4} emu/cm^3$. An NRM difference of the same magnitude, 2.3 times, but opposite sense, is observed when J stable value for the sheet; $8.1 \times 10^{-4} emu/cm^3$ is compared with J stable for the flow; $3.61 \times 10^{-4} emu/cm^3$. This result indicates that the stable NRM component in the sheet is of a higher intensity than in the flow unit. The NRM of the flow may be carried primarily by abundant fine-grained single or pseudosingle domain titanomagnetite which has a higher coercivity (i.e. higher remanence at J 200) but lower total remanence than the coarser grained titanomagnetite of the sheet.

3.2 NRM Intensity and Inclination

Inclination of the stable natural remanent magnetic moment changes six times over the length of the core interval as is shown in Figure 5. The relationship between inclination and NRM intensity between adjacent samples having opposite polarity is generally one of lower NRM intensity being associated with normal inclination (see Figure 6). This relationship is supported by consideration of the average magnetic intensity at both 200 Oe, J 200 and over the demagnetization range of the stable magnetic inclination, J stable. For normal inclinations, average J 200 for reverse inclinations is 2.5 times this value or 3.71×10^{-4}emu/cm^3 and for reverse inclinations, this parameter is 1.3 times the normal inclination value; 6.1×10^{-4}emu/cm^3.

Figure 6 shows that over the 60 cm to 210 cm core interval, consecutive samples hving a single NRM polarity also have relatively uniform J 200 values. Below and above this interval, there is a wide variation in J 200 values between samples having a single NRM polarity.

4. Results: Jo

4.1 Comparison with J 200

Variation of NRM intensity with demagnetization may be shown by a combined plot of Jo and J200. Jo is generally parallel to the J200 remanence profile as is shown in Figure 7. Many of the plotted J200 values are higher than J200. The higher J200 values reflect the addition of magnetic remanence to the samples through alternating field demagnetization.

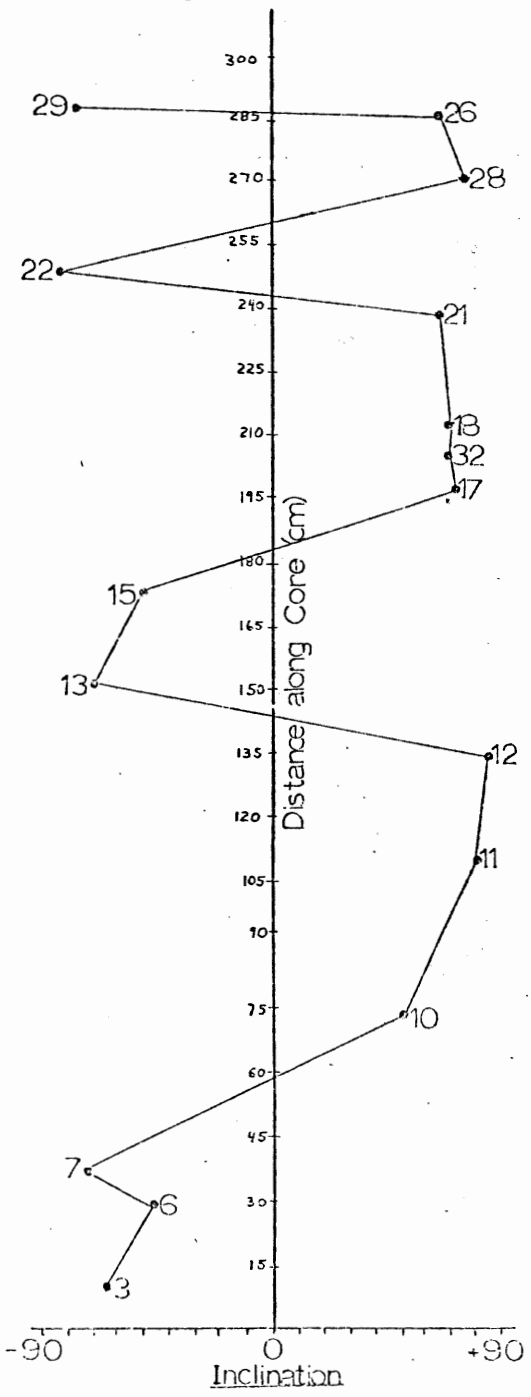

Figure 5. Plot of stable NRM inclination observed along core.

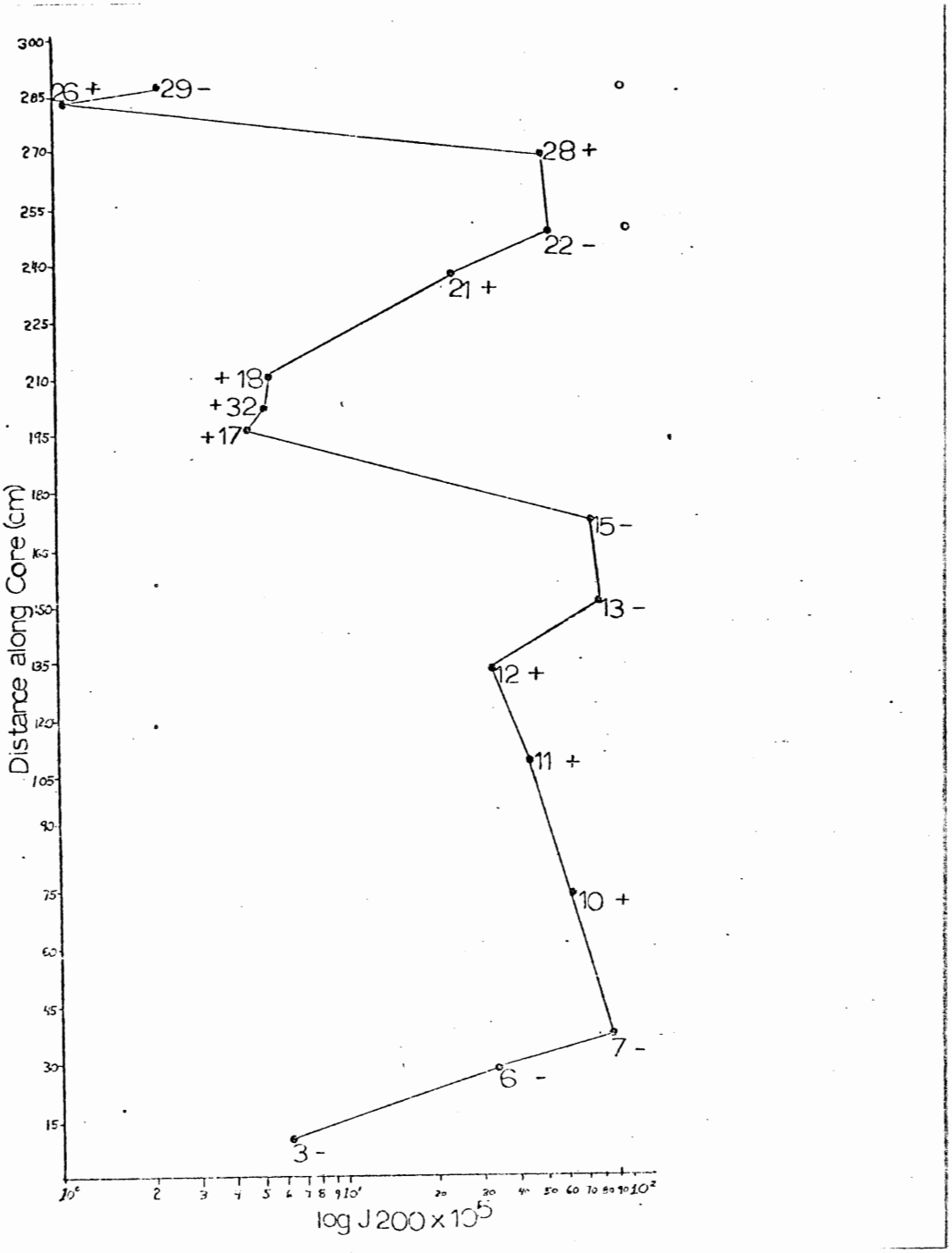

Figure 6. Plot of log J 200 x 10^5 versus distance along core. Stable inclination polarity of the samples is shown on the plot.

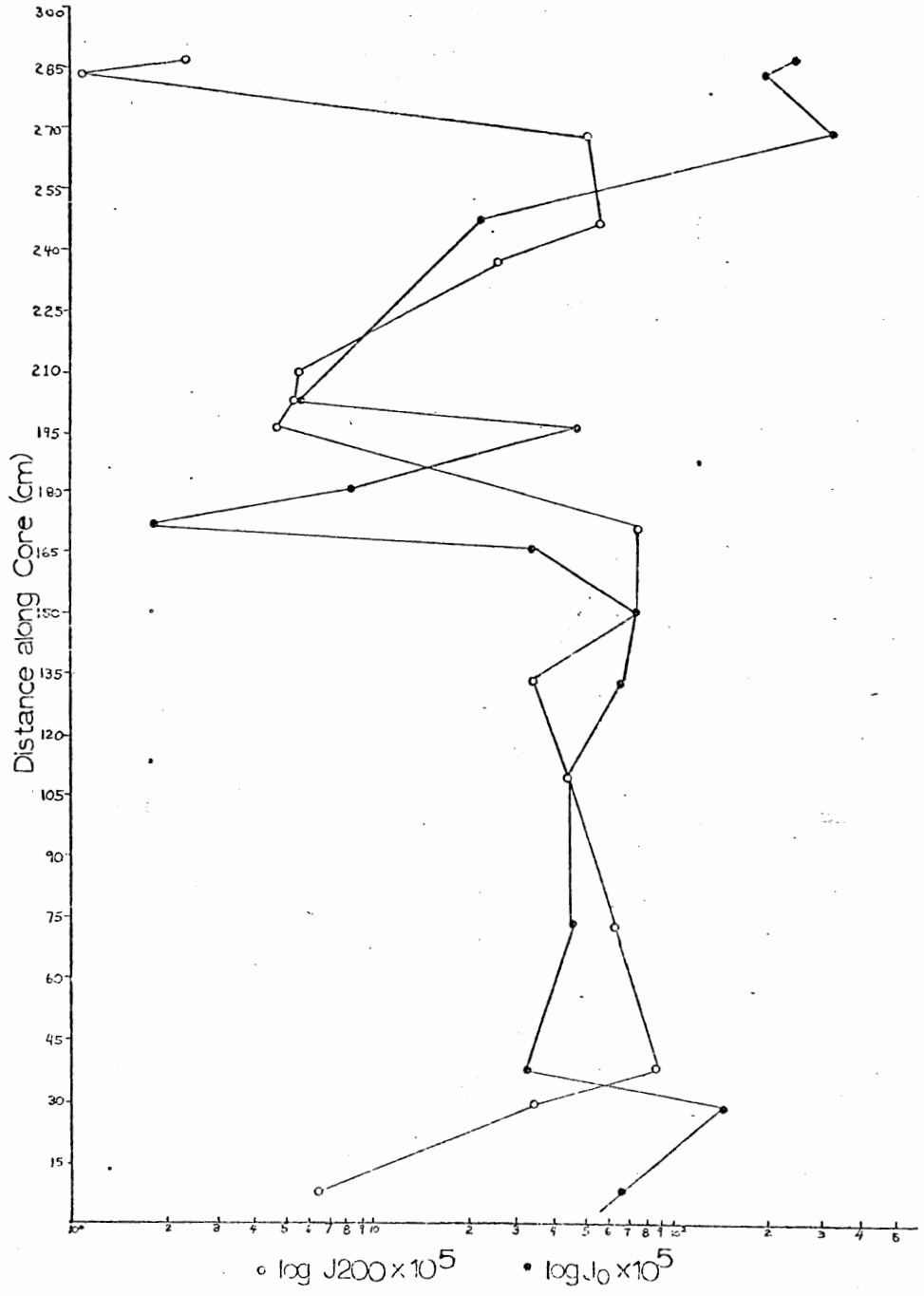

Figure 7. Plot of log J 200 x 10^5 and log J 0 x 10^5 versus distance along core.

In the breccia unit located through the upper 38 cm of the core, the Jo plot parallels the J200 plot with depth, but over the upper 30 cm of the breccia, the Jo magnetic intensity is larger by about 1.0 x 10^{-3}emu/cm^3. This secondary remanence is restricted to the breccia and is rapidly lost across the base of the breccia unit. Similarly, data from the basal 30 cm of the core indicates that Jo is larger than J200.

4.2 Drilling Induced Remanent Magnetization

Zijderveld diagrams for selected samples from the breccia unit and basal sheet, Samples 7 and 29, respectively, Figures 12a and 12e, show the removal of a large vertical downward directed magnetic component having a lower coercivity than the magnetic remanence associated with the stable inclination. This secondary magnetic component cannot be an insitu viscous moment since the ambient dipole geomagnetic field at Bermuda is aligned at +52°. It has been suggested by Rainbow et al. (1972) and Johnson and Ade-Hall (1975) that a strong but soft magnetic component of this type has been acquired during the drilling process and is aligned along the axis of the drill string.

5. Mean Demagnetizing Field

Alternating field demagnetization curves for selected core samples are shown in Figure 8. These curves have been normalized so that Jo equals 1.0 by dividing J at each demagnetization step by the J NRM value measured at zero demagnetizing field. Comparison of these plots shows that there is a wide variation in the decay of normalized moment with increasing alternating field demagnetization.

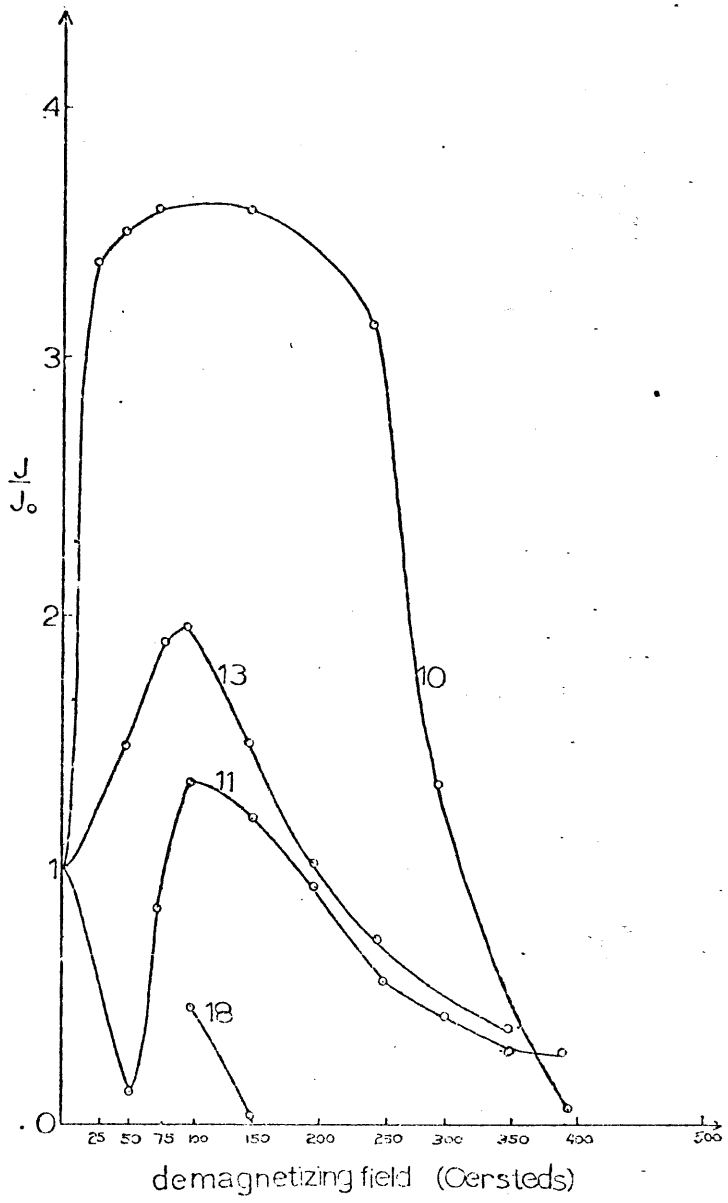

Figure 8. Selected alternating field demagnetization curves. Parts of the curves displaying highly irregular NRM intensity have been omitted and all curves have been normalized so that J/Jo equals 1 at the 0 oersted demagnetizing field level.

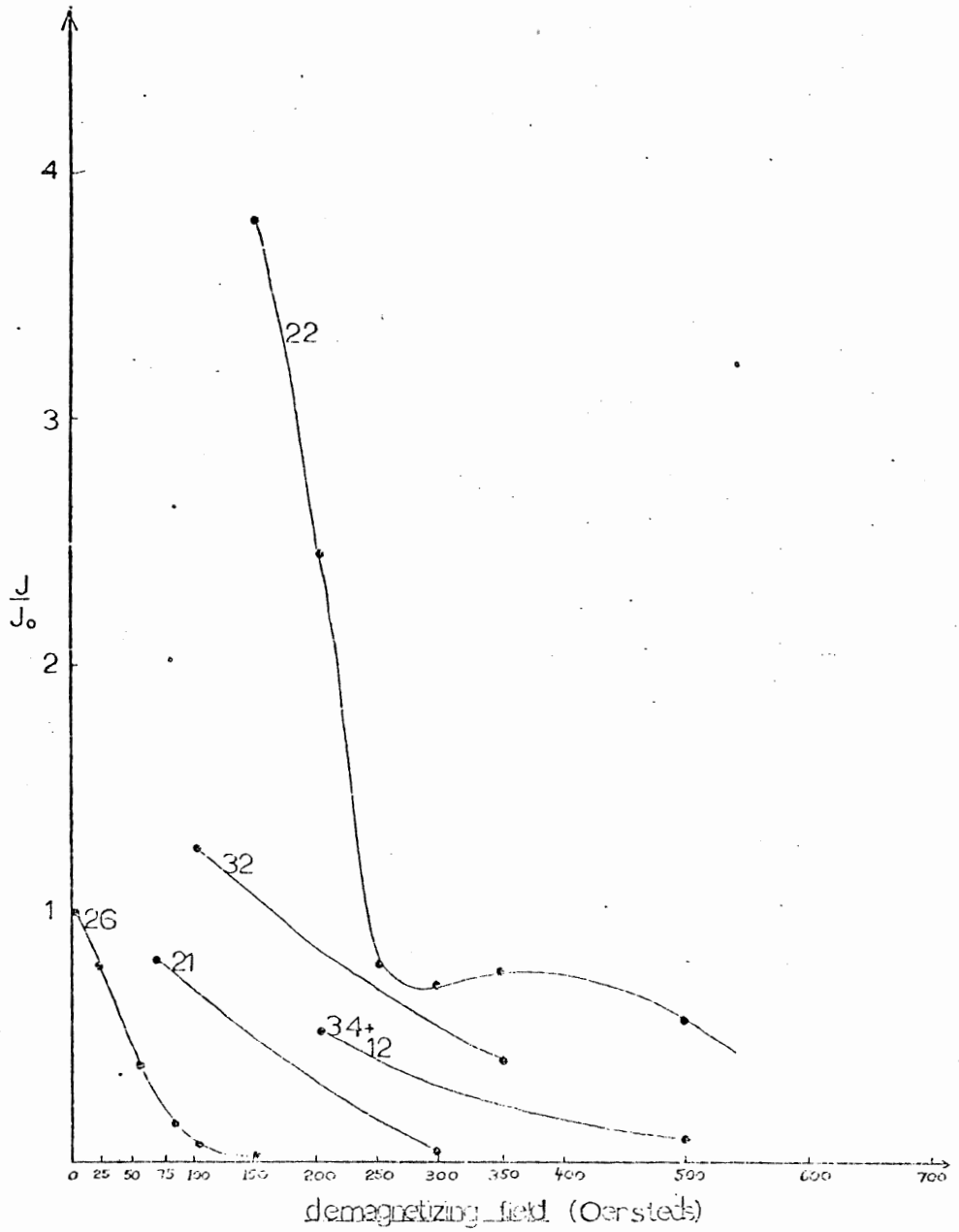
J/Jo
4
3
2
1
22
32
26
21
34+12
0 25 50 75 100 150 200 250 300 350 400 500 600 700
demagnetizing field (Oersteds)

Irregular normalized moments at demagnetization fields less than 100 Oe prevents accurate determination of the MDF intensity. Estimated MDF values obtained through graphical extrapolation range from 50 Oe to 300 Oe. MDF values in excess of 300 Oe have been observed in 34% of the DSDP basalts.

Normal pillow MDF should display values that are inversely proportional to grainsize and decrease toward the coarse grained flow interior (Ryall and Ade-Hall 1975). The variability of the observed MDF intensities results from differential low temperature alteration, bimodal grainsize distribution of the magnetic phase, and at the chilled margins, the formation of secondary magnetite or the conversion of hematite to magnetite.

6. Discussion of NRM Intenisty

The Bermuda core section samples have magnetic intensities that are about an order of magnitude less than the typical intensities reported for oceanic basalt. The average undemagnetized NRM intensity over the core interval is $2.61 \times 10^{-4} emu/cm^3$. Lowrie (1974) gives an average NRM intensity of $2.73 \times 10^{-3} emu/cm^3$ for a collection of DSDP basalt and Ryall et al. (1977) report a DSDP Leg 37 hole average NRM intensity of $3.7 \times 10^{-3} emu/cm^3$.

A larger difference in NRM intensity is observed when the Bermuda core intensities are compared to the magnetic remanence of unaltered pillow basalt. The magnetic characteristics of pillow basalts recovered from distances of 0, 10, and 25 km from the Mid-Atlantic Ridge have

been used by Ryall (1975) to model the magnetic intensities of pillows as a function of their distance from the spreading ridge crest. Average NRM intensity at 0 km from the axis is predicted to be 5.2 x 10^{-2}emu/cm^3 at 10 km from the axis, it is 1.5 x 10^{-2}emu/cm^3; and at 25 km from the axis, average NRM intensity is 2.1 x 10^{-3}emu/cm^3.

The lower remanence observed in the Bermuda core with respect to the Mid-Atlantic Ridge pillows suggests that the NRM is not the original thermal remanent magnetization required when the lava cooled.

Both flows and sheets are characterized by magnetite (580°C) Curie temperatures, and microprobe analysis has shown that most of the titanomagnetite must have phase split submicroscopically into a low and high titanium titanomagnetite fraction (Rice 1977). Frequently observed granulation textures are evidence of the phase separation process (Evans and Wayman 1974). Textural evidence such as spherulitic plagioclase in altered basaltic glass as well as the absence of deuteric alteration indicates that the phase splitting process was not an initial cooling feature. Rice et al. (1980) conclude that temperatures during a hydrothermal event associated with sheet intrusion (100°C to 200°C) were high enough to phase split the titanomagnetite grains.

The observed remanence of the Bermuda lavas is related to the formation of secondary magnetite or the conversion of hematite to magnetite during hydrothermal alteration concomitant with or subsequent to sheet intrusion. Secondary magnetite formation would not be

uniform since alteration through the circulation of hot seawater would be concentrated along interflow contacts and within flow fractures. In the pillow selvedges larger amounts of available Fe results in the formation of a higher volume of secondary magnetite in comparison to the pillow interior. The magnetic remanence acquired by the secondary magnetite is a fraction of the remanence it would have acquired had it cooled through its blocking temperatures from above the Curie point.

VI NATURAL REMANENCE POLARITY

1. Results: Inclination Dispersion Histograms

Inclination dispersion over the sequence of alternating field demagnetization steps has been analyzed using histograms, stereoplots and Zijderveld diagrams.

Figure 9 shows that the distribution of stable NRM inclinations is discontinuous with a sharply peaked upwards magnetized group having an average inclination of -65.6° and abroad, equally distributed downwards magnetized group with an average inclination of +69.6°.

Figure 10 is a series of inclination histograms showing the NRM inclination dispersion obtained from a 0.0 Oe to 500 Oe stepped alternating magnetic field demagnetization sequence. At a demagnetization field of 0.0 Oe the NRM inclinations are widely dispersed between -90° and +80° with most inclinations clustered between 0° and 85°. The average inclination over this interval is estimated to be in near agreement with the present average Bermuda dipole inclination of +52°. Demagnetization at 25 Oe results in dispersion of most inclinations between -90° and -20°. Between -40° and -30°, inclination frequency is six times greater than all other inclination frequencies over the -20° to -90° interval.

Figure 9. Stable NRM inclination histogram. Broken lines indicate average normal and reverse inclinations.

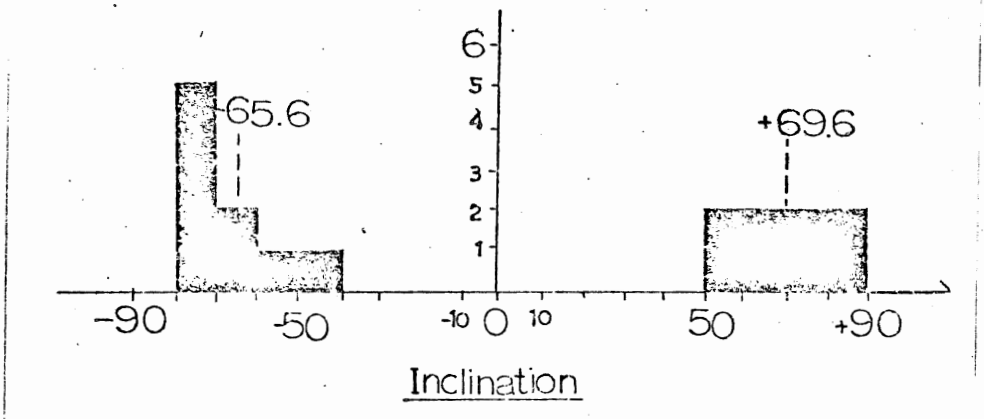
6
5
4
3
2
1
65.6
+69.6
-90
-50
-10
0
10
50
+90
Inclination

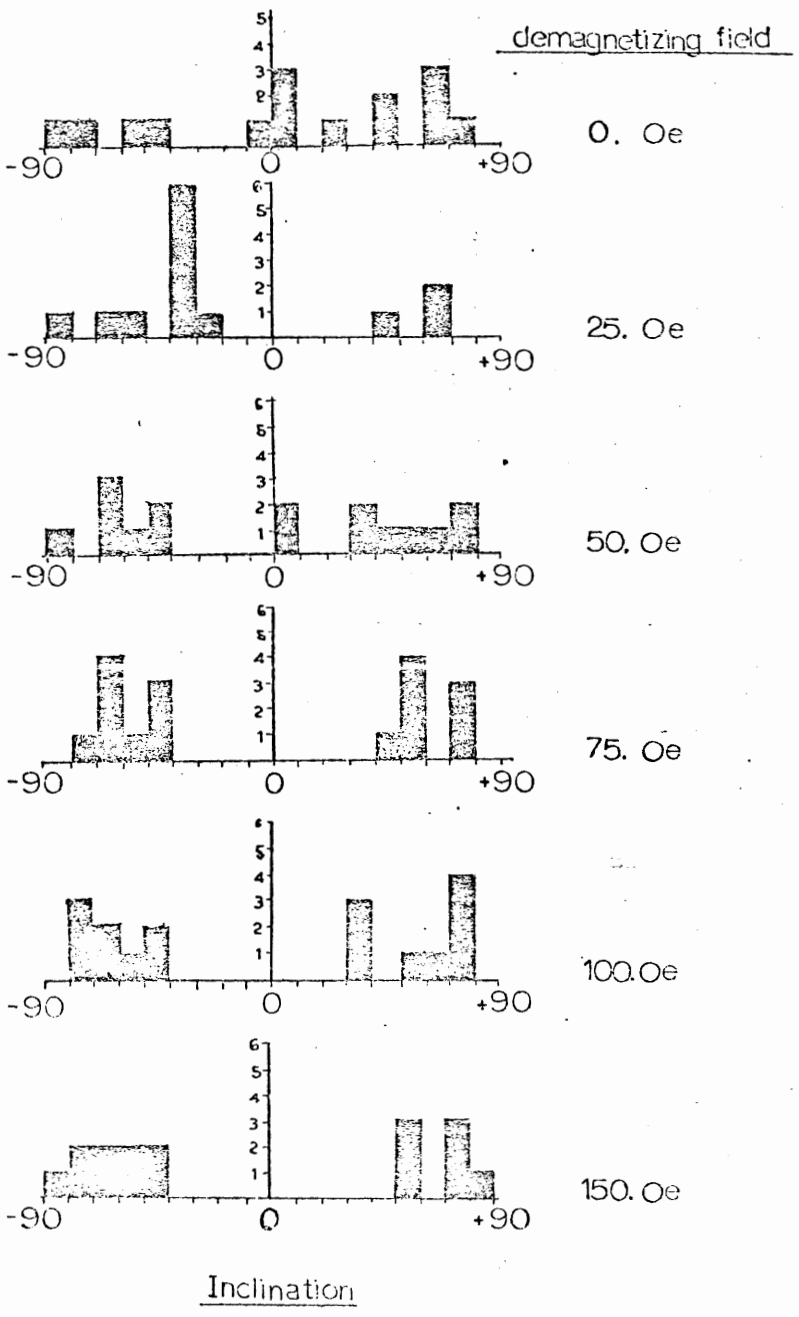

Figure 10. Histograms of inclination dispersion with alternating field demagnetization.

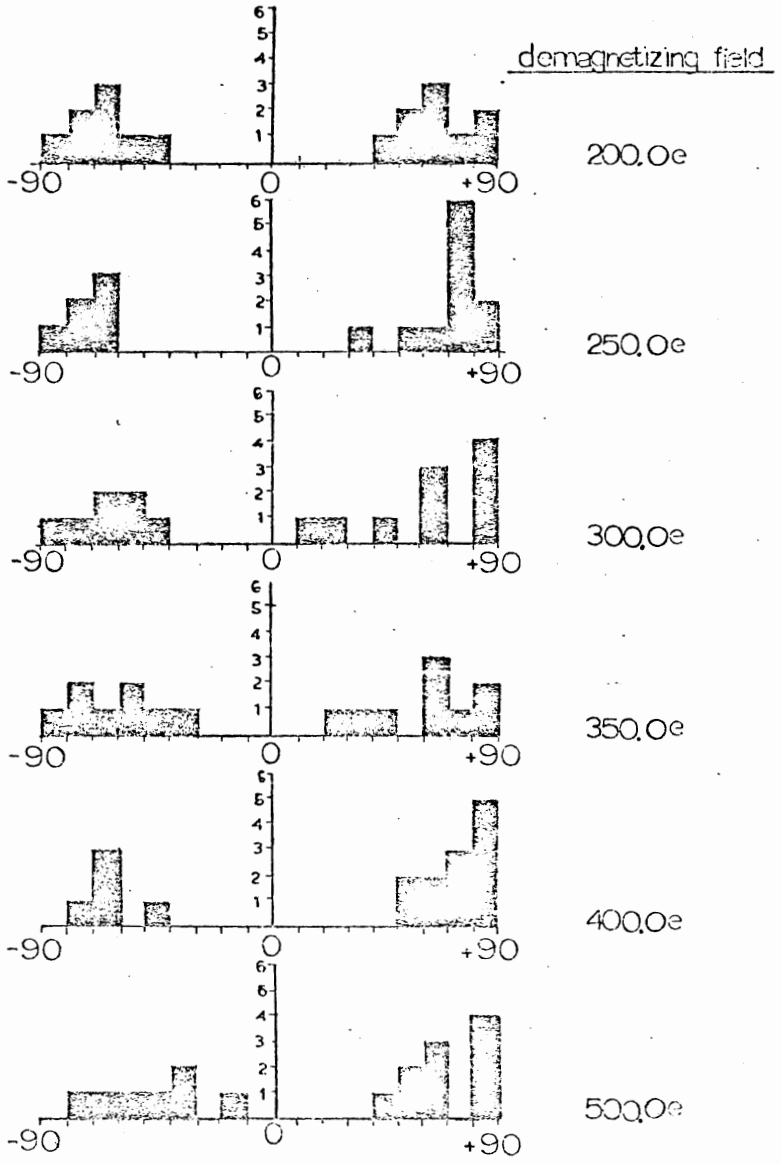
demagnetizing field
200.0e
250.0e
300.0e
350.0e
400.0e
500.0e
-90
0
+90
Inclination

Demagnetization at higher alternating field intensities produces a two-sided inclination dispersion pattern. The inclination frequency distribution appears most symmetric at the 200 Oe demagnetization field level where maximum, normal and reversed inclination frequency occurs between $\pm 60°$ and $\pm 70°$.

2. Results: Stereoplots

Representative demagnetization stereoplots are given in Figure 11. The stereoplots do not reveal any obvious demagnetization patterns. There are approximately an equal number of plots that show steepening and shallowing of inclination with increasing demagnetization. The change of inclination with demagnetization was very irregular for many samples: 32% of all samples did not yield a stable inclination.

3. Results: Zijderveld Diagrams

The points plotted in the Zjiderveld diagrams represent successive positions in orthogonal projection of the end point of the total magnetization vector during progressive demagnetization. This magnetization vector is plotted in a rectangular axis system in which the axes are the horizontal and vertical planes. Figure 12 is a series of Zijderveld diagrams from selected samples yielding stable inclinations and derived from the vertical, east and north components of the magnetic vector at each demagnetization step. Stable inclination values were obtained by taking a linear regression line through points that intersected or plotted close to the origin. In this respect, the vertical-east projection proved to

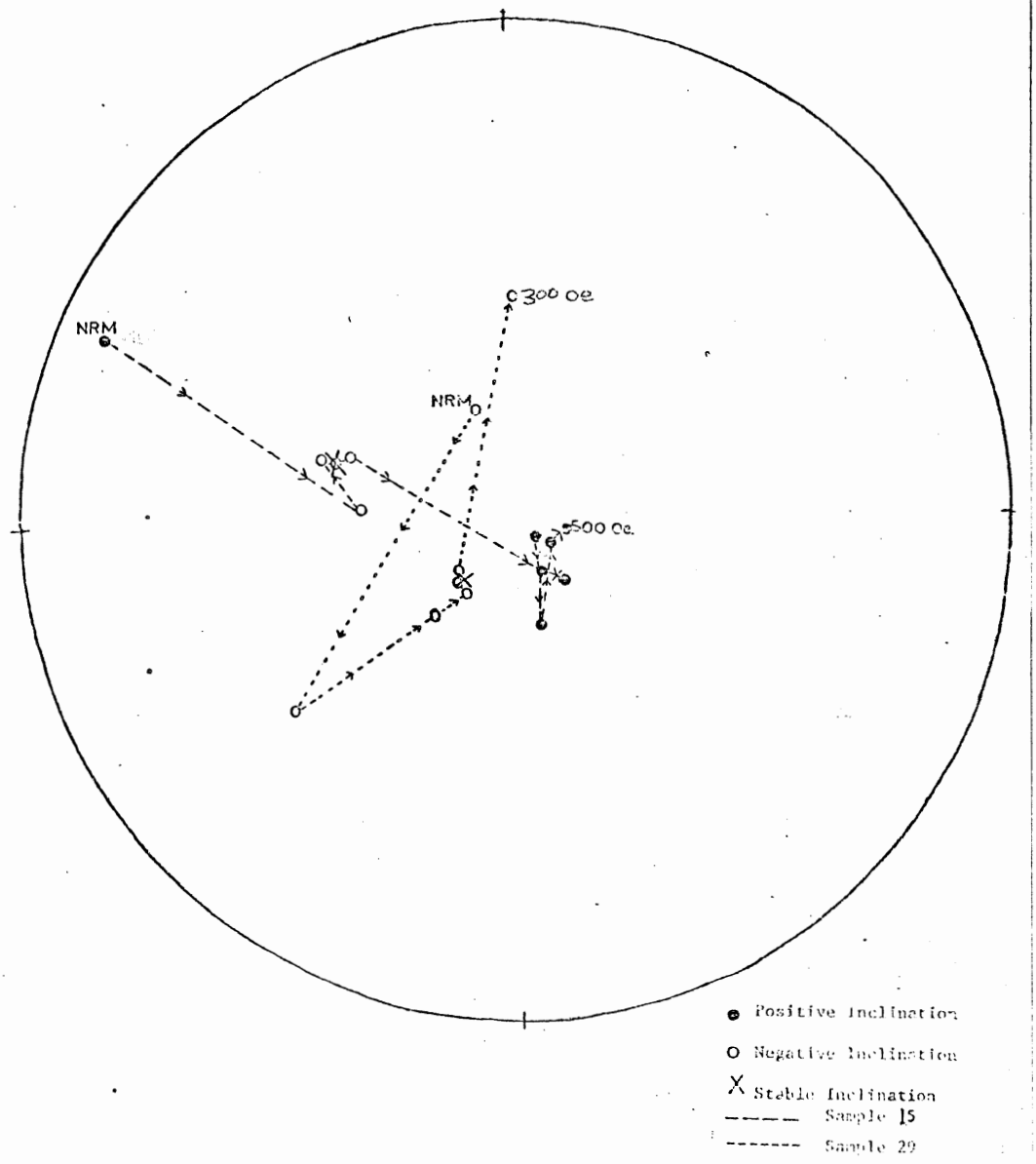

Figure 11. Selected sample demagnetization stereoplots. Declination of each sample is arbitrary.

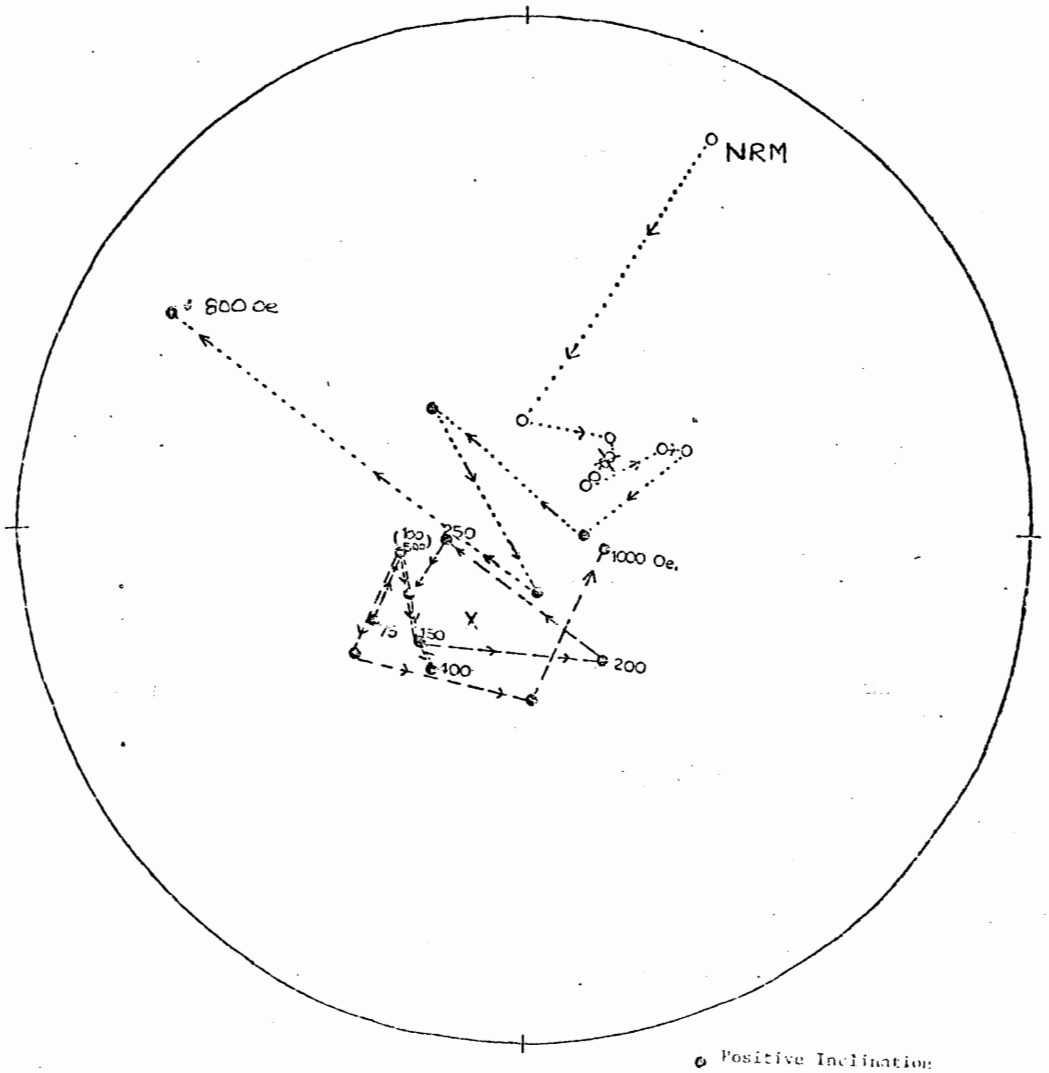

● Positive Inclination

○ Negative Inclination

× Stable Inclination

——— Sample 21

····· Sample 13

be most useful in all cases. A linear demagnetization trend may result from the demagnetization of a single magnetic vector (ie. the stable thermal remanent moment) or two magnetic vectors may be affected simultaneously. Linear trends that do not pass through the origin may be due to induced secondary magnetism or sample magnetic anisotropy (Zijderveld 1967).

The variation between inclinations derived from the selected Zijderveld plots and the stable inclination values ranges from 0.8% to 9.2% with an average variation of 5.2%.

3.1 Drilling Induced Remanence

Zijderveld plots for Samples 29 and 17, Figures 12a and 12F, show an initial upward movement of the magnetic vector over progressive demagnetization levels less than 50 Oe. The removal of a downward directed low coercivity magnetization component is indicated by these results. This strong by magneticly soft vertical component cannot be an insitu viscous moment since the present geomagnetic field at Bermuda is aligned at +52°.

It has been suggested (see for example: Rainbow et al. 1972, Johnson and Ade-Hall 1975) that a soft magnetic component of this type is a drilling induced remanent magnetization (DIRM) acquired during the drilling process and aligned along the axis of the drill string at +90°. A vector model (Figure 13) allows correction for DIRM if the insitu magnetization is considered to have the same inclination as the stable vector identified by partial demagnetization.

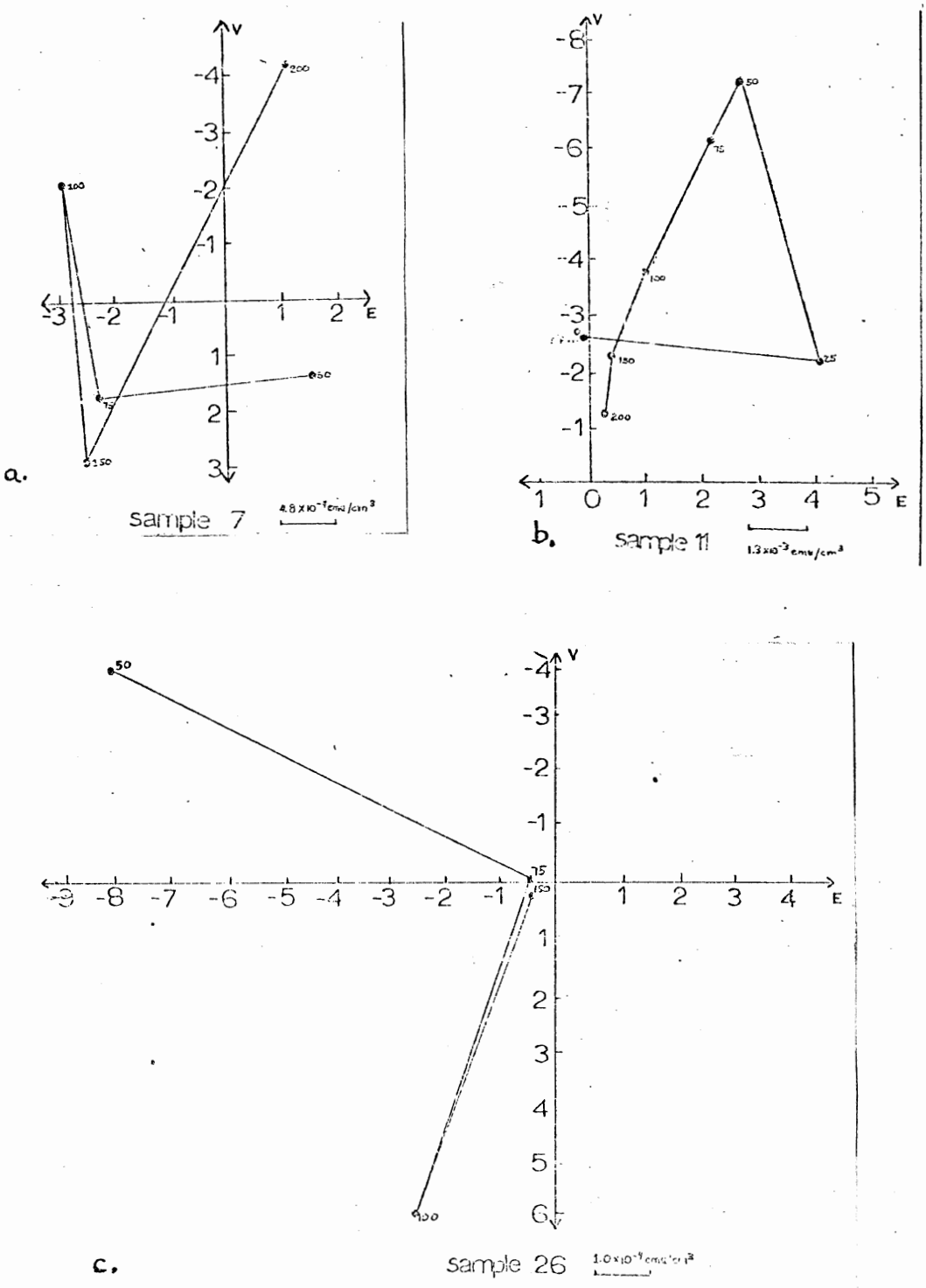

Figure 12. Selected sample Zijderveld Diagrams

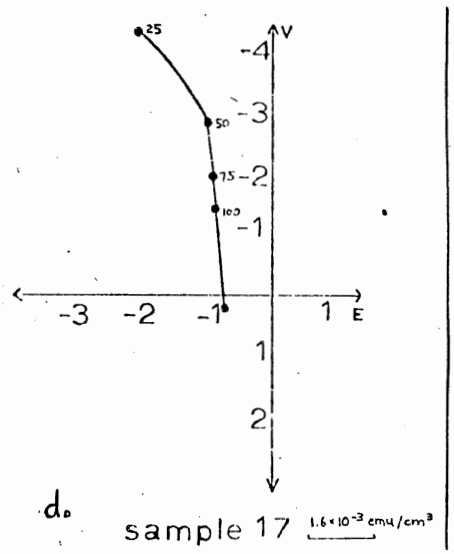

d. sample 17 1.6×10^{-3} emu/cm³

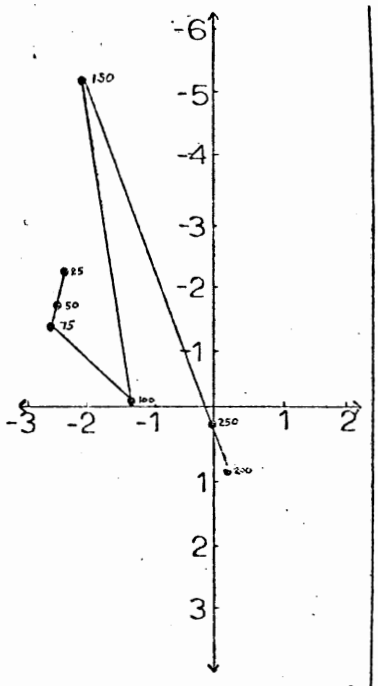

e. sample 32 2.0×10^{-4} emu/cm³

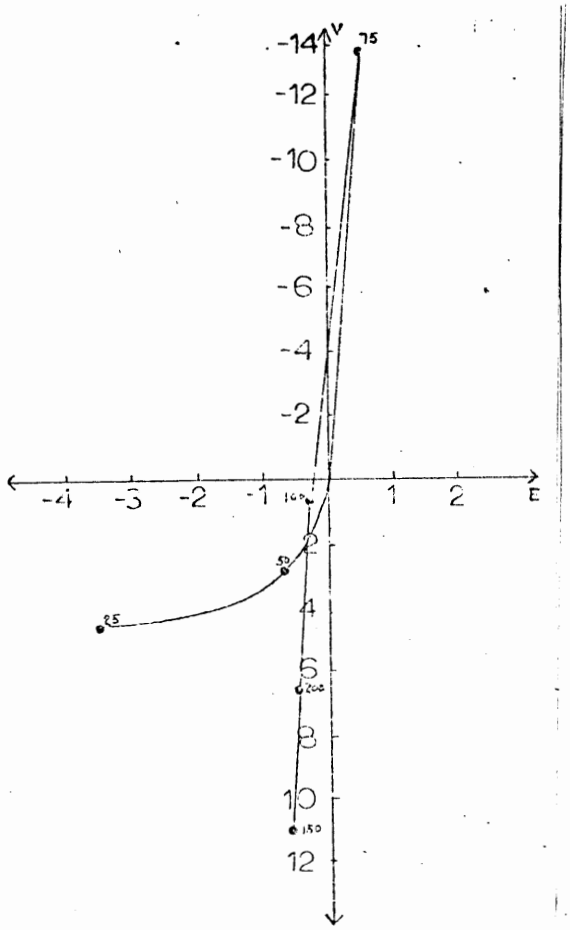

f. sample 29 1.1×10^{-4} emu/cm³

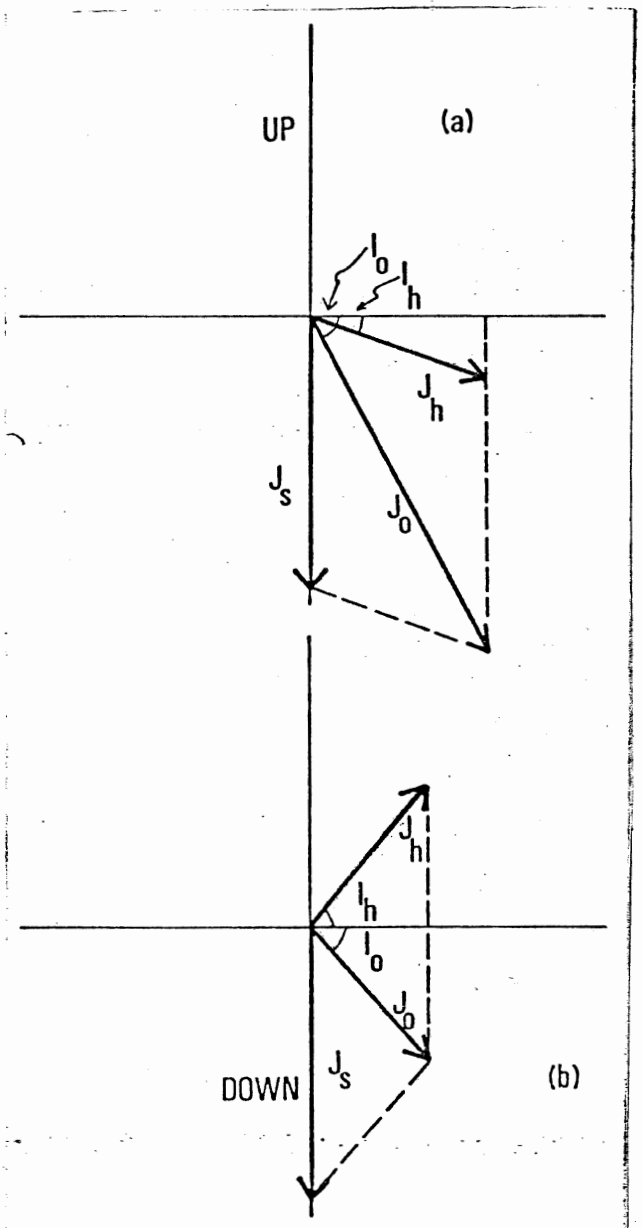

Vector model for soft and stable natural magnetization components of Bermuda flows and sheets: J_0 and I_0, intensity and inclination of natural remanence; J_h and I_h, intensity and inclination of stable component; J_s, intensity of vertically downwards oriented soft drilling induced component. (*a*) vector model for a downwards inclined stable component, (*b*) vector model for an upwards inclined stable component.

Figure 13. Vector model for drilling induced remanent magnetization (DIRM).
After: Rice et al. (1980).

The removal of a vertically downward directed DIRM component decreases the insitu NRM intensity of the downward magnetized samples and increases the insitu NRM intensity of the upward magnetized samples. An examination of low alternating field demagnetization trends for samples having initial normal and reverse polarity shows that demagnetization of samples having initial normal polarity increases the NRM intensity and demagnetization of samples having initial reverse polarity decreases the NRM intensity in agreement with the DIRM model.

The absence of well defined vertical DIRM components in the Zijderveld plots may be the result of the high degree of alteration throughout the core. Ade-Hall and Johnson (1976) state that DIRM is associated with unoxidized and coarse-grained (20 u) titanomagnetite. Grain cracking and granulation during hydrothermal alteration subdivides coarse-grained titanomagnetite and reduces effective grainsize so that the magnetic phases are less susceptible as carriers of drilling induced remanence.

4. Antiparallel Inclinations and Geomagnetic Field Reversals

The polarity of the stable demagnetized natural remanent magnetization changes six times over the length of the sampled core (see Figure 5 and Table 2). The angular difference at changes of inclination polarity averages 137°, and in all cases is over 120°. There is near antiparallel alignment of the average normal and reverse magnetic inclinations; +69.6° and -65.6°, respectively. These observations imply that the inclination distribution may be attributed to 180° reversals of the earth's magnetic field.

The highly fractured nature of the core precludes most comparisons of declination change associated with inclination reversals. The 123° change in inclination over the continuous core interval between Sample 7 and 10 is coupled with a 179° change in declination. This is an expected result for 180° reversals of the earth's field. Over the core intervals between Samples 21 and 22 and Samples 26 and 29, where the change in inclination is 144.8° and 139.3°, respectively, the corresponding changes in declination are 27.3° and 57.8°.

Although these results are not conclusive, they suggest that declination change associated with inclination reversal is closer to 180° or 0° than 90°. Rice et al. (1980) conclude that a 180° change in inclination may not be accompanied by a 180° change in declination, and inclination reversal without declination reversal may occur when normal, and reversed fields are of comparable intensity.

5. NRM Polarity of the Sheet

The correlation of positive inclinations and large remanence intensities for core sections having over 50% sheets has been observed by Rice et al. (1980). The core section in this study has intercalated normal and reverse inclinations. Over the basal 80 cm of the core, inclinations are consistently normal with the exception of two steep reverse inclinations. This result suggests that the flow unit and sheet have distinctive magnetic characteristics. The magneticly normal mid-Tertiary sheet intrusion event appears to be a magnetic overprinting in the flow unit where 66% of the stable inclinations have reverse inclination.

VII SUSCEPTIBILITY

1. Introduction: Equipment and Results

The total magnetic moment of a rock is the vector sum of the component Jin, induced by an external field (e.g. the earth's) and the moment of natural remanent magnetism (J NRM). The intensity of component Jin in a weak field H is given by: Jin = kH, where k is a constant of proportionality called susceptibility or initial susceptibility.

For small concentrations, susceptibility is directly proportional to titanomagnetite volume (Nagata, 1961). When grainsize is below 100 u, susceptibility varies with grainsize (for example: Parry, 1965). It varies inversely with low temperature oxidation (Ade-Hall, 1976) and titanomagnetite ulvospinel content (Nagata 1961).

Susceptibility was measured on a Minnetech Labs Model Ms-3 susceptibility bridge. The measured susceptibilities are given in Table 3 and are plotted against depth in Figure 14. Figure 15 is a histogram of susceptibility values.

TABLE 3. SUSCEPTIBILITY emu/cm^3. (Oe x 10^{-9})

SAMPLE NUMBER	SUSCEPTIBILITY
1	0.88
3	1.31
4	2.07
5	2.04
6	1.78
7	1.77
8	0.61
10	0.69
11	2.20
12	1.70
13	1.72
14	0.84
15	1.06
16	0.85
17	2.66
18	0.16
19	1.14
21	1.85
22	2.48
23	1.93
24	2.53
25	2.05
26	2.83

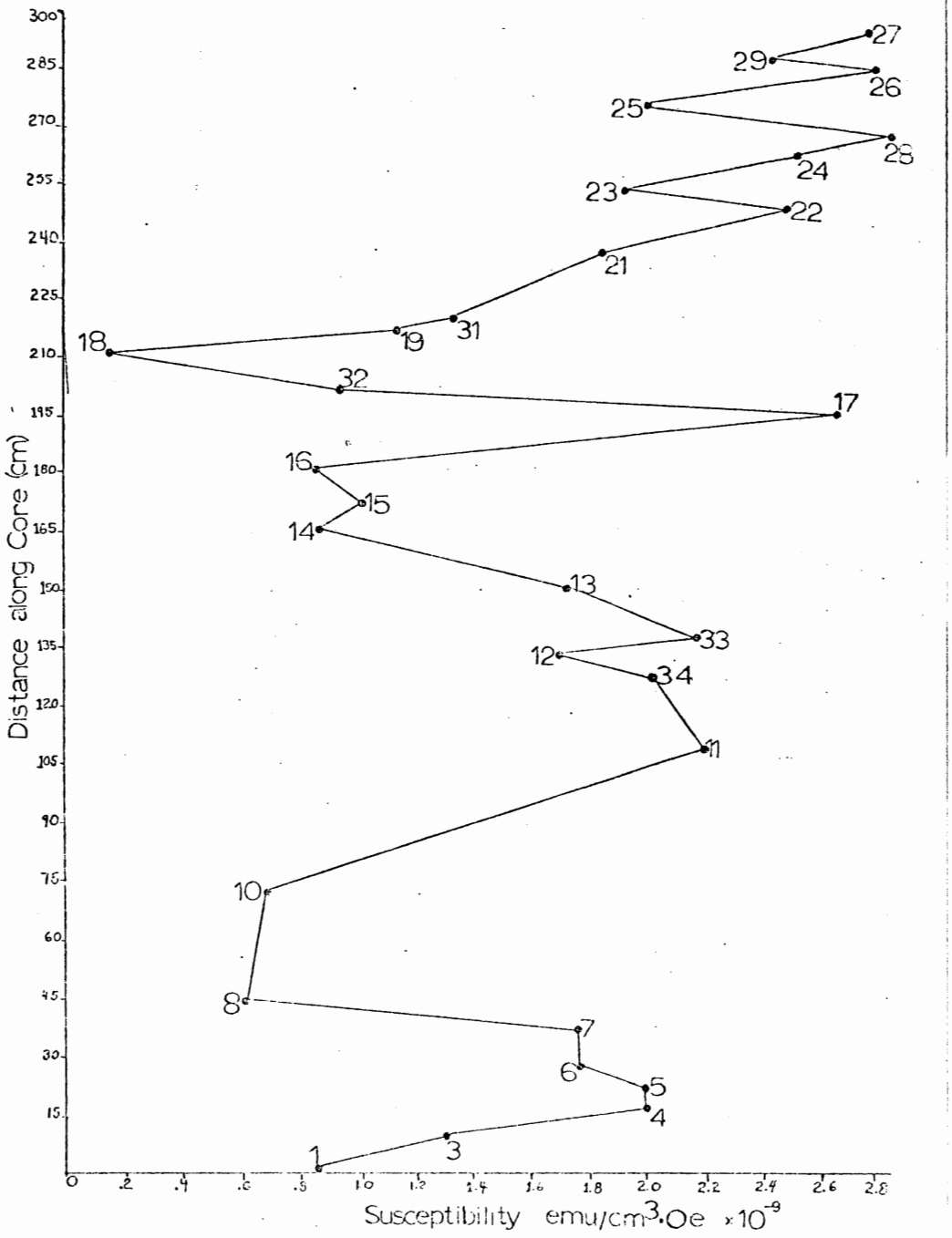

Figure 14. Plot of susceptibility versus distance along core.

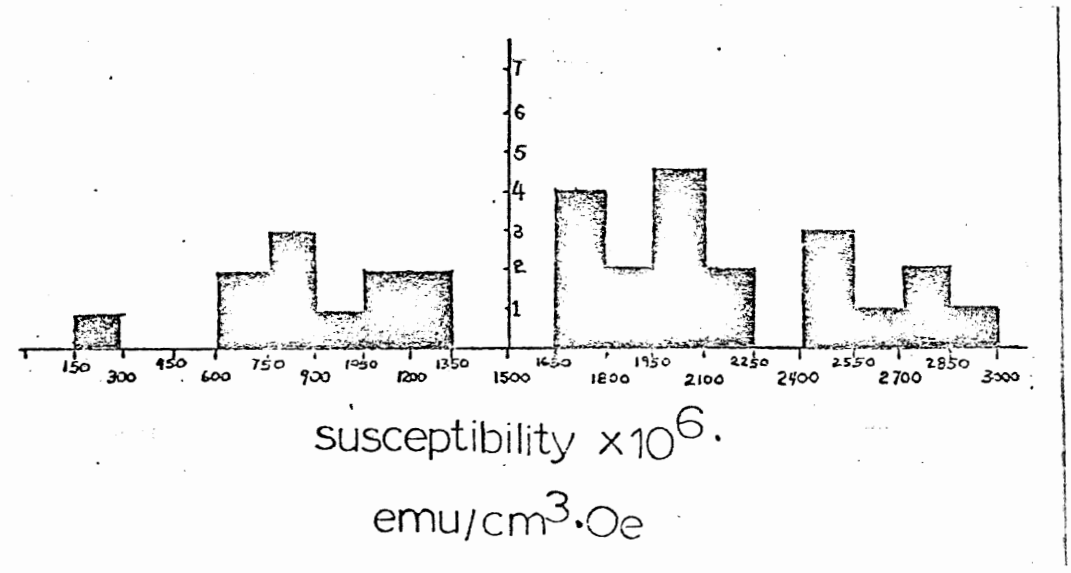

Figure 15. Susceptibility Histogram

3. Correlation of Susceptibility with Petrographic Observations

Throughout the length of the core section, petrographic data may be cited that supports the controlling influence of grainsize, titanomagnetite volume and degree of alteration on susceptibility maxima and minima distribution.

Between 0 and 30 cm, the increase in susceptibility is matched by a decrease in chloritization and an increase in opaque mineral concentration and grain size.
The reduction in susceptibility between 30 cm and 75 cm may be attributed to an initial reduction in titanomagnetite concentration. Other samples in this interval are from brecciated cooling units that have a high degree of chloritization and small grain sizes.

Samples from 108 cm to 150 cm have variable, but relatively high, susceptibilities. This interval is a flow unit with several minor breccia inclusions. Reduced grainsize, increased alteration at the flowbreccia contact and decreased titanomagnetite concentration between the breccia units controls the distribution of susceptibility minima.

Consistently low susceptibilities occur through the breccia interval between 165 cm and 180 cm. Samples from this core interval are highly altered and fine grained. There is a minor increase in susceptibility at the center of the breccia interval, suggesting larger grainsize and reduced alteration in this zone.

Sample 18, taken from a breccia flow contact, has the minimum susceptibility measured in the core section. Chlorite alteration is extensive and highly granulated to finely disseminated 10 u titanomaghemite, and titanomagnetite are the main opaque phases present.

The constant increase in susceptibility over the interval 213 cm to 240 cm reflects a gradational increase in grainsize and reduction in chloritization with distance into the basal flow unit.

The interval 240 cm to 297 cm has high, but variable, susceptibility values. Susceptibility minima are related to zones of reduced titanomagnetite concentration and increased alteration. The susceptibility minimum at Sample 23 may be associated with a chilled dike contact. A thin rapidly cooling intrusion would produce small-grained titanomagnetite and contribute to secondary alteration of pre-existing titanomagnetite, thereby reducing the susceptibility of these granulated grains. Similarly, the susceptibility minimum associated with a breccia inclusion at 280 m may be related to small grain size and increased alteration at the chilled breccia margin.

The average susceptibility of the sheet, the basal 80 cm of the core, is significantly higher than the average susceptibility of the remainder of the core which is considered to be a brecciated flow unit. Average flow susceptibility is 1.36 x 10^{-3}emu/cm^3, and average sheet susceptibility is 1.8 times this value or 2.44 x 10^{-3}emu/cm^3. These susceptibility values fall within the broad range of susceptibilites defined for

submarine basalt. Rice et al. (1980) have concluded that higher sheet susceptibility is primarily due to higher titanomagnetite volume. Grain alteration within the sheet probably reduces the effective grain size of the larger titanomagnetite grains to a size comparable to titanomagnetite of the flow unit.

4. Susceptibility and Mean Demagnetizing Field

Estimates of the mean demagnetizing field (MDF) for selected samples were obtained graphically from the plots of J/Jo versus demagneting field (Figure 8). MDF values may be used as a measure of magnetic hardness or coercivity of the NRM. MDF and hence coercivity is primarily controlled by the effective grain size which determines the single domain, pseudosingle domain or multidomain characteristics of the magnetic phase. Higher MDF values indicate a harder remanence that is carried by a magnetic phase having small effective grain size; ie. MDF (coercivity) is proportional to the inverse of the grain size (Parry (1955) and Dunlop (1973)). For grains having dimensions less than 100 u, susceptibility k varies with grain size (Parry 1965). Therefore, susceptibility varies with the inverse of the MDF.

The validity of the k x $^{1}/_{MDF}$ relationship was tested using the available MDF and susceptibility data. Samples or sample groups were ranked on a coercivity scale from 1; highest coercivity to 9; the lowest coercivity sample. Similarly, sample susceptibility was ranked from 1; lowest susceptibility to 12; the highest susceptibility sample or sample group (see Table 4).

TABLE 4. MDF AND SUSCEPTIBILITY RANKING OF SAMPLES

	MDF Rank	Sample(s)
High MDF	1	7
	2	10
	3	22
	4	13, 11, 32
	5	34, 12
	6	17
	7	21
	8	28, 29
Low MDF	9	26

	Susceptibility Rank	Sample(s)
Low Susceptibility	1	18
	2	8, 10
	3	1, 14, 16
	4	32, 15
	5	19
	6	3, 31
	7	6, 7, 12, 13
	8	4, 4, 34, 23, 25
	9	11, 34, 33
	10	26, 24, 22
	11	17
High Susceptibility	12	27, 29, 28

Coercivity rank was plotted against susceptibility rank, ie. $^{1}/_{MDF}$ versus k, as is shown in Figure 16. A linear regression line through the plotted data gives a correlation factor of 0.50.

A significant source of error in this analysis is the estimation of MDF values from incomplete graphical data. However, within the limits of the available data, the results indicate that the susceptibility, k, is proportional to the inverse of MDF.

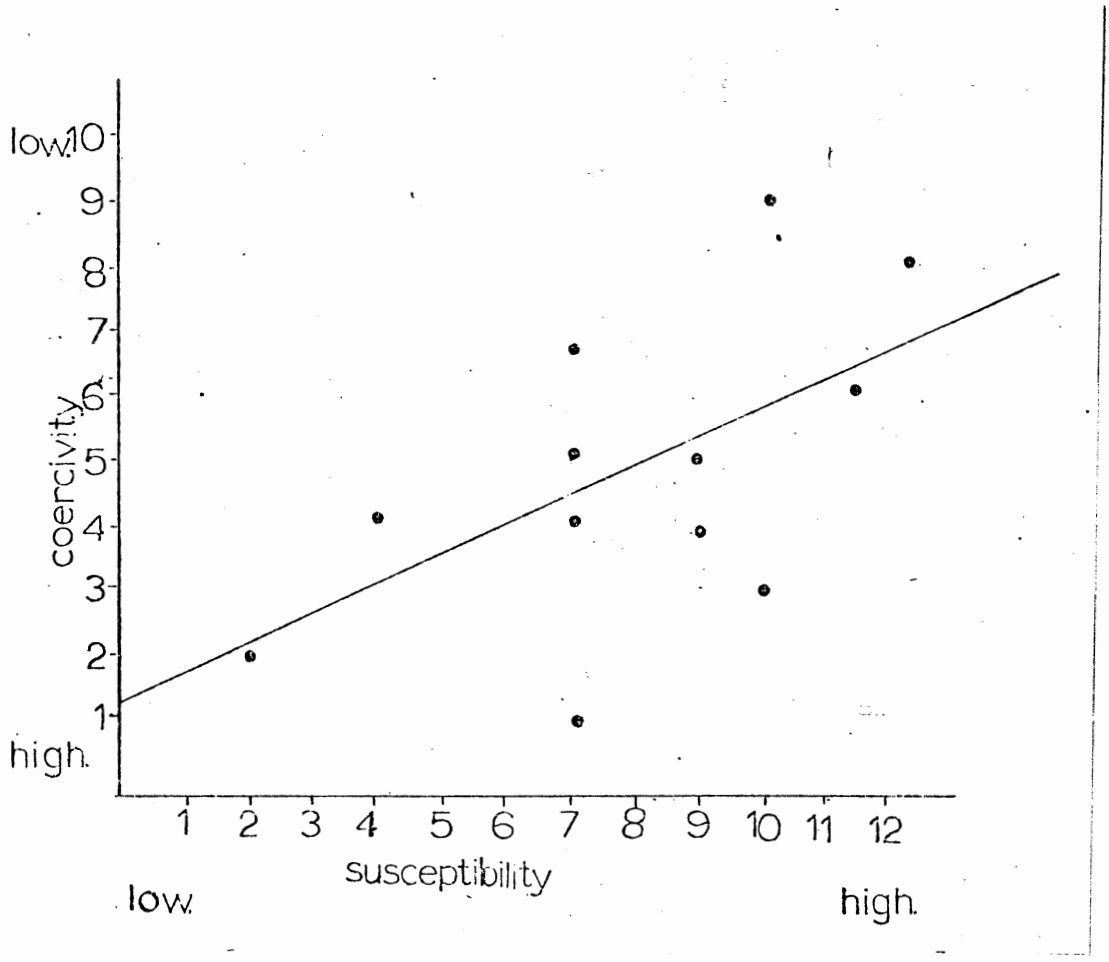

Figure 16. Plot of coercivity rank versus susceptibility rank

VIII OPAQUE MINERALOGY

1. Introduction: Methods and Titanomagnetite Classification

A Zeiss Ultraphot II was used to examine all sample thin and polished sections. The accuracy of volume, and grainsize trends and estimates is limited by the methods used in examining the sections. These limitations primarily arise from the small and varied grain size, the high degree of grain disintegration and the irregular distribution of the opaque phases within the samples.

The sample description and hydrothermal altration classification used is based on that given by Abdel-Aal (1977).

Titanomagnetite types are differentiated on the basis of grain size and habit. The classification is as follows:

Titanomagnetite type 1: large euhedral to subhedral grains larger than 20 u that frequently have peripheral corrosion.

Titanomagnetite type 2: fine to medium euhedral grains, 5 u to 20 u.

Titanomagnetite type 3: 5 u to 18 u grains similar to type 2, but they have experienced rapid cooling and hence have a skeletal form.

The hydrothrmal alteration classification given by Abdel-Aal (1977) and used in polished section description is as follows:

1. Low degree hydrothermal alteration

   class L1: Homogenous titanomagnetite

   L2: Lines of grey-white titanomaghemite in titanomagnetite. This is accompanied by volume change cracks.

   L3: Small patches of titanomaghemite develop in titanomagnetite. Total patch area is less than 50% of the grain area.

   L4: More than 50% of the grain area, or the entire grain is changed to titanomaghemite.

2. Medium degree hydrothermal alteration

   M1: L4

   M2: Titanomaghemite is altered to anisotropic white, highly reflective titanohematite. Titanohematite occurs as spots replacing titanomaghemite or as small inclusions in the titanomagnetite.

   M3: Titanohematite transforms to a granule phase rich in $T;O_2$. The width of pre-existing cracks may increase and a dark brown to black phase (sphene) is formed. The granulated areas occupy less than ½ the area of the original titanomagnetite.

   M4: The granulated areas now include whole grains and the dark brown to black sphene spreads throughout the grain.

2. Summary of Observations

The following is a summary of opaque mineralogical observations through the core section. Complete polished section descriptions are given in Appendix 3.

Most titanomagnetite observed shows extensive alteration. Type 2 titanomagnetite; 5 u to 20 u euhedral to subhedral grains predominate and some subhedral to euhedral type 1 titanomagnetite grains occur. The alteration ranges from patchy titanomagnetite replacement by titanomaghemite to grain boundary and internal cracking with varying degrees of granulation alteration. Grain cracking and granulation limits the effective grain size in most grains and altered porphyroclasts to 5 u or less. In all sample descriptions, the maximum grain size is given. Most opaque grains were finer than 10 u and contain a large number of grains in the size range of 1 or 2 u.

The core intervals between 0.11 m and 0.31 m (polished sections 4, 5 and 6) and between 1.62 m and 1.89 m (polished sections 14, 15 and 16) consist of breccia that is highly chloritized and cut by calcite filled veins and fractures. There is a bimodal opaque grain size distribution throughout each of these brecciated zones, suggesting multistage crystallization. Titanomagnetite and titanomaghemite phenocrysts (40 u to 70 u) occur in a highly altered matrix, and most grains have irregular and cracked grain boundaries with minor granulation alteration. Titanomagnetite phenocrysts frequently have patchy titanomaghemite inclusions and partial granulation along grain boundaries. In some

instances granulation alteration involves the complete phenocryst, resulting in highly altered phenocryst remanents while in other grains granulation is limited to internal cracks and the grain boundaries.

The center of the breccia zones are less chloritized than the breccia margins. Phenocrysts of titanomagnetite and titanomaghemite are more granulated and unaltered titanomagnetite less abundant at the breccia margins than in the breccia interiors. In all samples examined, more than one degree of alteration occurs.

An indistinct grain size gradation pattern may occur in the breccia zones. The base of the breccia has a reduction in titanomagnetite and titanomaghemite concentration and grain size relative to the upper and middle breccia zones where titanomagnetite grain size and concentration increases downward.

Breccia zones partially cut and are separated by lava flows that range in thickness from 4 cm to 75 cm. Polished sections taken from the breccia-flow contact have a bimodal titanomagnetite-titanomaghemite grain size distribution. Grainsize ranges from 4 u to 12.5 u with 70 u to 100 u phenocrysts. Alteration ranges from titanomagnetite with patchy titanomaghemite inclusions to partial and complete phenocryst granulation.

The opaque mineralogy observed between stratigraphicly successive flow and breccia units is illustrated by polished sections 7 and 8. Type 2, 10 u, titanomagnetite predominates in both flow and breccia. Limited type 1 titanomagnetite and granulated porphyroclasts up

to 40 u occur in the flow. Average titanomagnetite grain size decreases to 5 u within the breccia where alteration ranges from partial titanomaghemite replacement to partial and complete grain granulation. Matrix alteration is most concentrated in areas depleted in titanomagnetite. Titanomaghemite grain size distribution is bimodal; 5 u to 3 u titanomaghemite grains occur with highly granulated 10 u tp 15 u phenocrysts.

The core section below 2.13 m is lithologically distinguished by a lava sheet. Grain size coarsens slightly with depth from 10 u to 40 u, and groundmass alteration is minor throughout.

The upper contact of the sheet has subhedral to anhedral 10 u titanomagnetite. Most titanomagnetite grains have cracked grain boundaries with minor granulation. Within the sheet, 20 u to 40 u titanomagnetite and titanomaghemite occurs. The concentration of these minerals shows a general decreasing trend toward the bse of the sheet, and grain size increases toward the center of the sheet. The titanomagnetite displays a range of titanomaghemite replacement, internal cracking and granulation. Highly granulated titanomaghemite porphyroclasts and a decrease in titanomagnetite concentration is associated with the breccia zone at 2.75 m. Titanomagnetite grainsize increases to 40 u to 70 u at the base of the sheet where most grains are cracked and have varying degrees of granulation. White, highly reflective anhedral to subhedral titanohematite occurs as inclusions and as discrete grains.

Sulfide mineralization was not common in the core samples examined. Where present, the sulfide phases occurred as discrete and very finely disseminated grains that had yellow-white to blue color in reflected light.

IX FLOW SUMMARY: NRM INTENSITY, SUSCEPTIBILITY AND OPAQUE MINERALOGY

Correlation of NRM and susceptibility profiles with specific petrographic and mineralogical characteristics is difficult due to the superposition of two or more grain size and compositional generations in the magnetic phase and the variability of the degree of alteration throughout the core.

General trends evident from this type of correlation suggest that the NRM intensity is variable through the brecciated flow margins that are situated above and below a massive flow unit located over the 30 cm to 160 cm depth interval. The central 35 cm of core from this flow unit is missing. Jo and J 200 profiles (Figure 7) indicate that the NRM intensities are relatively constant through the flow, and NRM increases into the basal sheet.

Opaque phase volume and grain size trends correlate with the observed Jo profiles through the brecciated pillow flow margins. Both Jo and J 200 increase with depth over the 10 cm to 35 cm core interval. The concentration of opaque minerals increases with depth throughout the margins. Grainsize coarsens toward the center of the brecciated margin. Susceptibility and J profiles are similar through the upper one-half of the margin. These results indicate that these magnetic parameters

are controlled to a significant degree by the volume of the magnetic phase. Over the lower one-half of the margin, a general similarity is retained between k and J profiles, but variations between profiles imply that grain size as well as the volume of the magnetic phase controls the magnetic properties.

The pillow margin between 162 cm and 189 cm has a symmetric Jo profile with a prominent central intensity minimum. Concentration of the opaque phase increases with depth, and there is a slight increase in grain size toward the center of the unit. The dissimilar susceptibility and J profiles indicates that grain size may act as a control of NRM. The increased susceptibility at the center of the unit correlates with observed coarsening of grain size.

Samples from the inter-pillow margin flow unit have a bimodal opaque concentration distribution. Samples 8 and 10 have opaque mineralogical contents of 10% and less than 5%, respectively, and grain coarsens slightly with depth over the same interval. At the base of the flow unit, samples 12 and 13 show that the concentration of the opaque phases decreases from 15% to less than 5% and grain size coarsens over the interval.

The flow unit has a relatively constant NRM profile suggesting that changes in magnetic intensity associated with reduction in magnetic phase concentration is compensated by larger grain size particles. Susceptibility profiles within and between the flow unit intervals correlate with the observed volume and grain size trends. The larger grain size of the lower flow interval (samples 12 and 13) may produce the higher susceptibility of this part of the core relative to the upper flow interval.

The high NRM intensities in the basal sheet are consistent with observations by Rice et al. (1980) that the sheets have higher oxide volumes and saturation magnetization values than the flow units.

With the available MDF data, Figure 16 shows that susceptibility, k, varies with the inverse of MDF. This is an expected result since MDF is lower and k higher where grain size and volume of the magnetic phase increases. For small concentrations, the volume of the magnetic phase is the primary control of susceptibility. As with NRM profiles, variations in MDF cannot be related to petrographic observations.

X PALEOMAGNETIC MODEL

Stable inclination vectors observed over the core interval are plotted in Figure 17. The diagram shows that the scatter of normal inclinations is greater than that of reverse inclinations. The average reverse inclination is -65.6°, and the average normal inclination is +69.6°. The near agreement of average, normal and reverse inclination vectors indicates that they represent sets of antiparallel inclination vectors that were possibly acquired during a period of magnetic field reversal when average dipole inclination was about ±68°. Conclusive declination information relating to inclination reversal is not available from the flow due to frequent fracturing of the core.

The eight reversely magnetized vectors clearly have a bimodal inclination dispersion. Six of these vectors are relatively closely grouped between -65° and -78° with an average inclination of -70.1°. The remaining two vectors have an average inclination of -50.7° with a relative inclination difference of 5.7°.

The nine normal magnetic vectors have an approximately equal dispersion between +52.7° and +85.2°. The average normal inclination of +69.6° is in near agreement with the predicted geomagnetic field inclination of ±68°.

Figure 17. Plot of all stable inclination vectors measured over the core interval. The inclination of the broken line is the predicted inclination of the reversing dipole which represents the mean inclination of the average normal and average reverse inclinations.

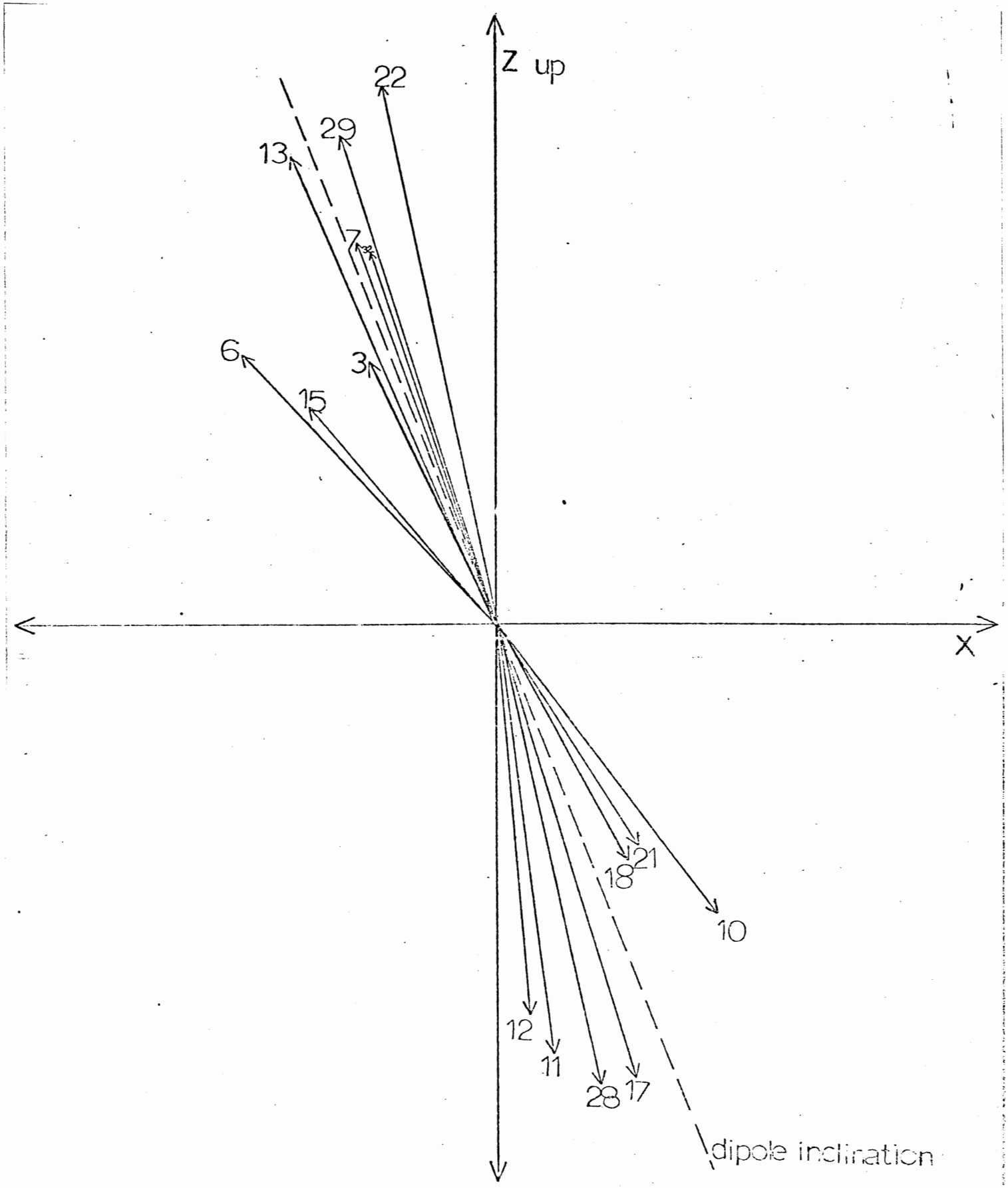
Z up
X
22
29
13
7
6
3
15
21
18
10
12
11
28
17
dipole inclination

The dispersion of normal and reverse magnetic vectors gives the following antiparallel vector pairs:

Reverse	Normal	Inclination Difference
22	28	180.4°
29	17	179.3°
13	16	178.9°
32	34	180.0°
7	34	180.8°

The low magnetic intensity normal inclination vector 26 may be the resultant of several combinations of vectors. Possible vector additions giving vector 26 are: 10+15, 17+32 or 17+7. It is not known whether the stable inclination of sample 10, 52.7° reflects the mid-Tertiary geomagnetic field at Bermuda predicted by Phillips and Forsyth (1972) to be $\pm$51°.

The inclination of samples 22, 29 and 13 have high NRM intensities. These high NRM reverse inclinations are from samples that are stratigraphicly below a series of normally magnetized samples. Similarly, samples 28 and 17 have high NRM normal inclinations and are stratigraphicly below reversely magnetized samples. These results suggest that changes of magnetic field polarity may be associated with high NRM intensity. Alternatively, the NRM of these antiparallel inclinations may be the result of less altered secondary magnetite which has a high intensity remanence acquired during a period of frequent field reversals.

The inclinations of samples 15 and 16, -47.8° and -45.9°, respectively, and the inclinations of samples 11 and 12, +82.9° and +85.2°, cannot be directly related to a primary geomagnetic field having antiparallel vectors with an inclination of ±68°. However, the inclination of both of these sample pairs may be related to the primary antiparallel field if they are considered as the resultant vectors of primary antiparallel magnetic moments and a secondary moment. Figure 18 shows the geometric relationship between these magnetic vectors. The normal and reverse components of the primary field are assumed to have equal intensities. The secondary moment has an inclination of +38° and an intensity of 7.2×10^{-6} emu/cm^3.

A model of this type for the Bermuda lavas has been suggested by Ade-Hall et al. (1973). Their conclusion is that the cleaned remanence of the lavas consists of two groups of antiparallel vectors representing initial thermoremanent magnetization acquired during a period of frequent field reversals during the late Palogene. The shallow normal secondary component is a thermo-chemical remanence probably acquired during the uniformly high hydrothermal alteration which has affected the lavas and distinguishes them from most other submarine flow material.

In summary, results from this examination of the Bermuda core shows that four vector pairs have antiparallel inclinations and are narrowly dispersed in relation to the assumed inclination of ±68° for the frequently

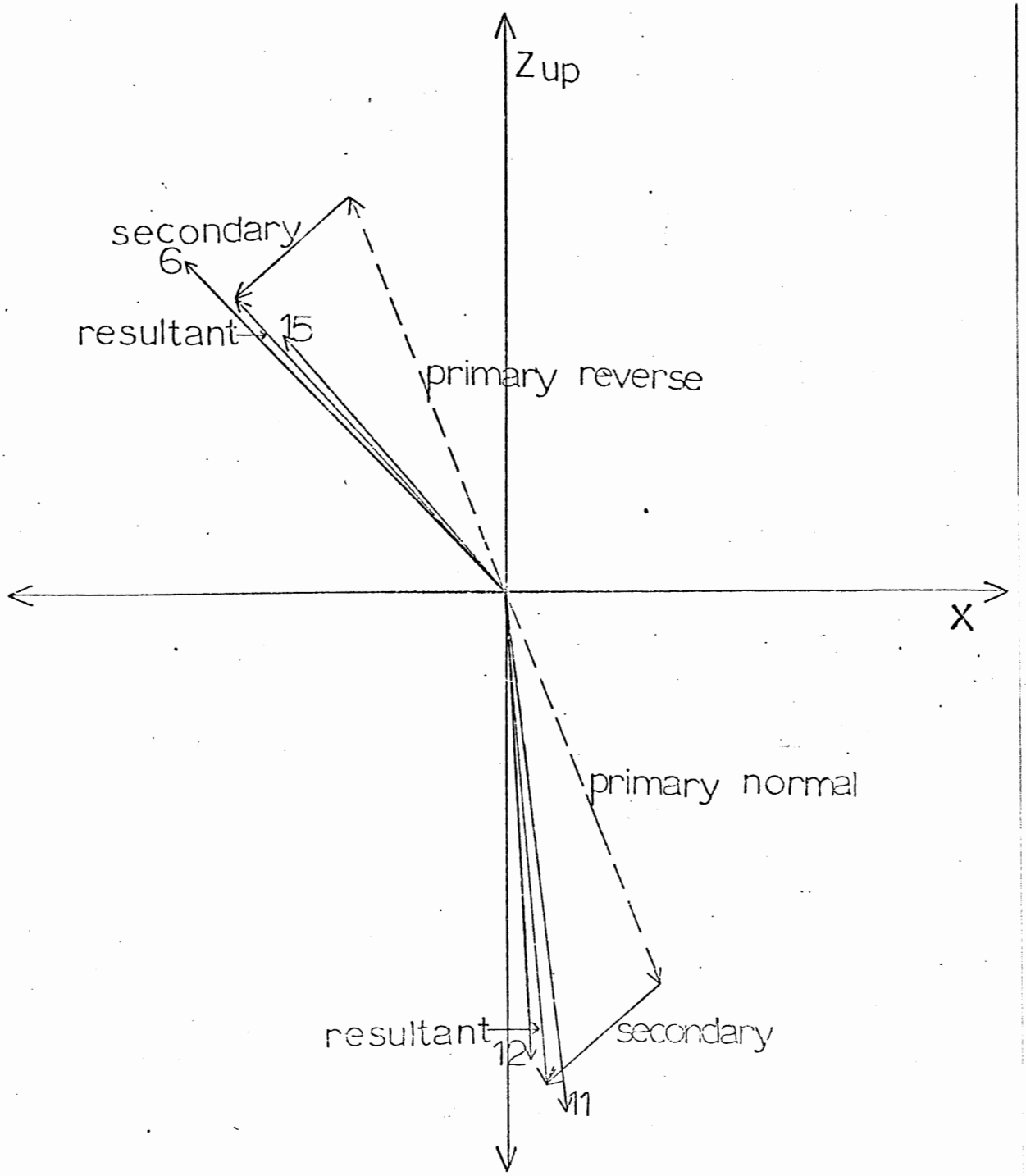

Figure 18. Paleomagnetic Model. Resultant vectors are averages of their respective plotted sample vectors.

reversing late Paleogene geomagnetic field. Two other vector pairs: 14 and 6 and 12 and 11, are the resultant vectors of the primary antiparallel moments and a secondary stable shallow chemical remanent magnetization.

As well as antiparallel inclinations, a frequently reversing geomagnetic field would be expected to have relatively uniform normal and reverse field intensities. Results from this flow unit conflict, in some respect, with these expected geomagnetic field characteristics. The scatter of normal inclinations is greater than that for reverse inclinations. Secondly, the J stable intensity for reverse inclinations is 1.4 times that for normal inclinations. At J 200, a demagnetization level after stable inclinations are achieved, this intensity difference increases to a factor of 2.4 times.

The high J stable and J 200 intensities for samples having reverse inclinations may be a grain size effect. Within the pillowed flow, where 75% of all negative inclinations occur, the grainsize of the titanomagnetites (10 u) is smaller than that in the sheet (10 u to 20 u). The flow unit titanomagnetite grains would be expected to have a lower remanence on an intensity per grain basis but higher coercivity than the grains that occur in the sheet. When compared to the magnetic grains of the sheet unit, the flow grains retain a higher remanence per unit volume, and less NRM is lost with alternating field demagnetization. The dispersion of normal inclinations may be due to the variability of within flow hydrothermal and thermo-chemical alteration processes. Presumably, this variability would result in polyphase formation of secondary magnetite that would magnetically record secular magnetic field variations and tectonic adjustment within the lava pile during or subsequent to the mid-Tertiary intrusive event.

None of the inclinations within the core interval are representative of the Cretaceous and mid-Tertiary inclinations at Bermuda which are predicted by Phillips and Forsyth (1972) to be -42° and +51°, respectively. In a more extensive study of the Bermuda core, Rice (1977) states that the original Cretaceous reverse magnetization has been overprinted by a single normal midTertiary magnetization during sheet intrusion. Rice et al. (1980) conclude that the inability to resolve the original stable magnetization components is the result of both magnetic components being held in nearly pure magnetite of similar grain size. The original Cretaceous reverse remanence is held by magnetite formed by phase splitting of the primary opaques while mid-Tertiary normal magnetization is held by magnetite formed by the decomposition of ferromagnesian silicates.

XI REVIEW OF RESULTS AND CONCLUSION

The rock and paleomagnetic character of a 3.0 m core interval consisting of a pillowed lava flow and basal intrusive sheet that was taken from a depth of 776 m in an 802 m core drilled on the Bermuda Seamount has been described.

The pillowed flow consists of brecciated pillow margins having spherulitic to cryptocrystalline plagioclase textures in a highly chloritized vitrophyric matrix. Hyalopilitic to intersertal plagioclase in a vitreous matrix occurs at the center of the flow unit. The basal sheet consists of fine to medium grained non-porphyritic holocrystalline basalt.

Within the flow unit type 2 titanomagnetite predominates with less abundant titanomagnetite phenocrysts and skeletal grains. The sheet is characterized by type 1 titanomagnetite. Extensive alteration, ranging from grain cracking to titanomaghematization and granulation, limits the effective grainsize in most titanomagnetite grains to 5 u or less.

The lower average NRM intensity of the Bermuda lavas when compared with Mid-Atlantic Ridge pillow basalts may be attributed in part to halmyrolytic and hydrothermal alteration processes. The primary magnetic remanence of

the flow unit is not the original thermo-remanent magnetization but is carried by secondary magnetite formed at sub-Curie point temperatures during hydrothermal alteration associated with the mid-Tertiary intrusive event.

A contrast in NRM intensity between the flow and the sheet unit has been observed. It is probable that the higher J stable remanence of the sheet when compared to the flow unit is due to the larger magnetic phase volume in the sheet while the lower J 200 magnetic intensity of the sheet reflects the lower coercivity of its relatively coarse-grained magnetic phase in comparison to the fine-grained (10 u) and skeletal titanomagnetite that occurs in the flow. Reverse inclination J stable intensities are approximately equal to normal inclination J stable intensities while J 200 intensities for reverse inclinations are 2.5 times the J 200 intensity for normal inclinations. This contrast in J 200 values reflects the higher coercivity of titanomagnetite within the flow where 75% of all stable reverse inclinations occur.

With the methods used in this study, the results of section V show that grain size cannot be regarded as the only factor controlling MDF. Factors other than magnetic phase volume control susceptibility. The extent of alteration and the nature of the magnetic phase composition will influence these magnetic parameters. It is known that MDF increases with the degree of oxidation, and susceptibility increases with titanomagnetite volume and decreases with both the extent of oxidation and the amount of ulvospinel produced through phase splitting.

There is a correlation of positive inclinations having high J stable magnetic remanences with the basal sheet. Two-thirds of all stable normal inclinations occur within the sheet. This fact, and the intercalation of reverse and normal inclinations in the pillowed flow suggests that, in its simplest form, the model for the magnetization of this lava involves the combintion of the primary Cretaceous reverse magnetization and a mid-Tertiary normal addition associated with sheet intrusion (Rice 1977). Anomalously shallow reverse and steep normal inclinations may be explained as the result and magnetic vectors of the primary field's estimated anti-parallel ($\pm$68°) magnetic moments and a secondary shallow, normal, chemical remanent magnetization.

Curie temperature anaylsis (Rice 1977) indicates that the original Cretaceous reverse and the mid-Tertiary normal inclinations cannot be separated since the magnetic remanence of both components is held in nearly pure magnetite of similar grain size. The elevated temperatures associated with the intrusive event results in granulation alteration and phase splitting of the previously oxidized titanomagnetite grains. These processes may magneticly overprint the original stable NRM so that most representative NRM directions will be carried by the interior of the units, not the altered chilled margins. The chilled margins of pillows and flows may also rotate while the interior of the cooling units retain plastic characteristics. This would produce a randomization of inclination across the differentially cooling igneous unit, with the more stable interior giving a remanence closer to the actual insitu inclination. Other possible sources for the observed inclination

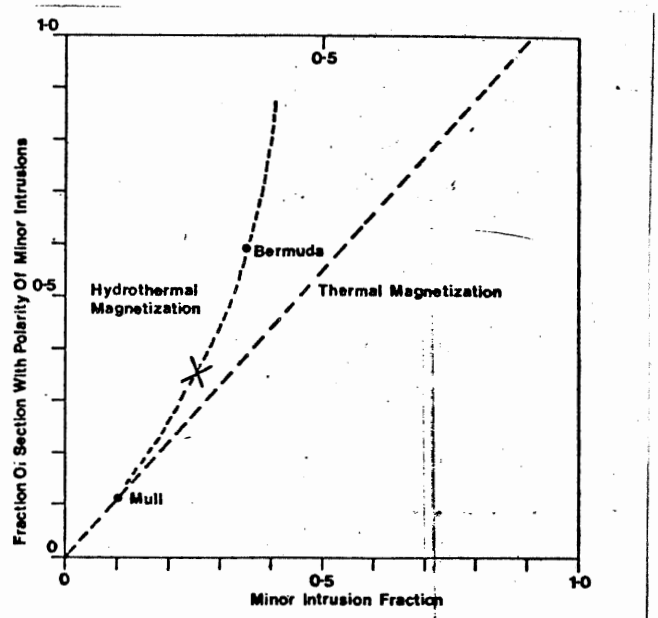

FIG. 13. Effectiveness of remagnetization by hydrothermal and thermal mechanisms.

Figure 19. Effectiveness of remagnetization by hydrothermal and thermal mechanisms. "Bermuda" denotes the results of Rice et al (1980) and X denotes the results of this study. Modified after Rice et al (1980).

dispersion include the polyphase formation of secondary magnetite which may record secular variations in the geomagnetic field. Tectonic adjustment of the lava flows and pillow margins during initial cooling or during the mid-Tertiary intrusive event and similarly, the subsidence and tilting of major volcanic constructional features within the seamount may also account for the inclination scatter.

Rice et al. (1980) have used the Bermuda core results and the results from field studies of thermal remagnetization at lava contacts of dykes to predict and compare the effectiveness of hydrothermal and thermal remagnetization processes in terms of the minor intrusion fraction and the fraction of the section with the polarity of the intrusives. Their results are shown in Figure 19. The relationship between variables is speculative but shows that hydrothermal remagnetization is more efficient in terms of the volume of rock acquiring a new magnetic direction than is thermal remagnetization. Results from this study of the Bermuda core (Figure 19) agree with the predicted relationship between variables for hydrothermal magnetization.

The magnetic complexity of the core interval may be related to the effects of high temperature alteration, tectonic adjustment and subsidence at depth within the seamount. Hydrothermal alteration, the production of secondary magnetite having low magnetic intensity, intercalation of normal and reversed inclinations and tectonic modification within the core reduces the effective magnetic intensity. These factors probably contribute to the low effective magnetization observed

in the North Atlantic where crustal drilling of the upper 600 m of oceanic basement has penetrated relatively strongly magnetized basalt. Rice et al. (1980) have concluded that remagnetization of the type seen in the Bermuda Seamount could produce a magnetic anomaly source zone of low intensity in the upper part of the sheeted dyke layer which lies at a depth below that sampled by DSDP drilling.

REFERENCES

Abdel-Aal, O. 1977. The alteration of opaque minerals and the magnetization and magnetic properties of volcanic rocks in a drill core from an active geothermal area in the Azores, Unpublished Ph.D. thesis, Dalhousie University, Halifax, N.S.

Ade-Hall, J.M., and Johnson, H.P. 1976. Paleomagnetism of basalts, Leg 34. In Initial reports of the Deep Sea Drilling Project, Vol. 34, R.S. Yeats, R.S. Yeats, S.R. Hart et al. United States Government Printing Office, Washington, DC, pp.513-532.

Ade-Hall, J.M., Lowrie, W., Opdyke, N.D. et al 1973. Deep Drill 1972; The Paleomagnetism of a Long Succession of Submarine Lavas From Bermuda (abst.) Eos (Am. Geophys Union, Trans.) Vol. 54, No. 4, p.486.

Aumento, F., Mitchell, W.S., and Fratta, M. 1976. Interation betwen sea water and oceanic layer two as a function of time and depth--1. Field evidence. Canadian Mineralogist, 14, pp.269-290.

Aumento, F., Ade-Hall, J.M., and Keen, M.J. 1975. 1974-The year of the Mid-Atlantic Redge. Reviews of Geophysics and Space Physics, 13, pp.53-66.

Aumento, F., and Ade-Hall, J.M. 1973. Deep Drill, 1972. Petrology of the Bermuda Drill Core (abst.) Eos (Am. Geophys. Union, Trans.) Vol. 54, No. 4, p.485.

Aumento, F., and Gunn--------1974. Deep Drill, 1972. Petrology of the Bermuda Seamount. Unpublished manuscript.

Dunlop, D.J. 1973. Thermoremanent magnetization in submicroscopic magnetite. J. Geophys. Res. 78, pp.7602-7613.

Evans, M., and Wayman, M. 1974. An investigation of the role of ultra-fine titanomagnetite intergrowths in paleomagnetism. Geophys. J. Royal Astro., 36, pp.1-10.

Evans, J.E. and Wayman, M.L. 1970. An investigation of small magnetic particles by means of electron microscopy. Earth and Planet. Sci. Lett., 4, pp.142-146.

Gees, R.A., and Medioli, F. 1970. A continuous seismic survey of the Bermuda Platform. Part I: Castle Harbour. Maritime Sediments, 6, pp.21-25.

Johnson, H.P., and Ade-Hall, J.M. 1975. Magnetic results from basalts and sediments from the Nazca Plate. Nature (London), 257, pp.471-473.

Larson, R.L., and Hilde, T.W.C. 1975. A revised time scale of magnetic reversals for the Early Cretaceous and Late Jurassic. J. Geophys. Res., 80, pp.2586-2594.

Lowrie, W. 1974. Oceanic basalt magnetic properties and the Vine and Matthews hypothesis. Geophys. J. Royal Astro. Soc., 40, pp.513-536.

Marshall, M., and Cox, A. 1972. Magnetic changes in pillow basalt due to sea floor weathering. J. Geophys. Res., 77, pp.6459-6469.

Nagata, T. 1961. Rock Magnetism. Maruzen Company Ltd., Tokyo, 350pp.

Parry, L.G. 1965. Magnetic properties of dispersed magnetite powder. Phil. Mag., 11, pp.303-1312.

Phillips, J.D., and Forsyth, D. 1972. Paleotectonics, paleomagnetism, and the opening of the Atlantic. Bull. Geo. Soc. of Am., 83, pp.1579-1600.

Rainbow, R.R., Fuller, M., and Schmidt, V.A. 1972. Paleomagnetic orientation of borehole samples. EOS, Trans. Am. Geophys. Union, 53, 355p.

Reynolds, P.R., and Aumento, F.A. 1974. Deep Drill 1972: Potassium-argon dating of the Bermuda drill core. Can. J. Earth Sci., 11, pp.1269-1273.

Rice, P. 1977. The Bermuda Seamount--an investigation into the magnetic properties and the $^{40}Ar/^{39}Ar$ radiometric age of selected hydrothermally altered submarine flows. M.Sc. thesis, Dalhousie University, Halifax, N.S., 219p.

Rice, P.D., Hall, J.M. and Opdyke, N.D. 1980. Deep Drill 1972: A paleomagnetic study of the Bermuda Seamount. Can. J. Earth Sci., 17, pp.232-243.

Ryall, P.J.C. 1974. A comparison between natural and laboratory oxidation of titanomagnetite in pillow lavas. Unpublished Ph.D. thesis, Dalhousie University.

Ryall, P.J.C., and Hall, J.M. 1979. Laboratory alteration of titanomagnetite in submarine pillow lavas. Can. J. Earth Sci., 16, pp.496-504.

Ryall, P.J.C., and Ade-Hall, J.M. 1975. Radial variations of magnetic properties in submarine pillow basalt. Can. J. Earth Sci., 12, pp.1959-1969.

Ryall, P.J.C., Hall, J.M., Clark, J., and Milligan, T. 1977. Magnetization of oceanic crustal layer 2--results and Thoughts after DSDP Leg 37. Can. J. Earth Sci., 14, pp.684-706.

Ryall, P.J.C., and Ade-Hall, J.M. 1975. Radial variations of Magnetic Properties in Submarine Pillow Basalt. Can. J. Earth Sci., 12, pp.1959-1969.

Schenk, P.E. 1973. Deep Drill 1972: Pleistocene stratigraphy. EOS, Trans. Am. Geophys. Union, 54, 486p.

Smith, B.M. and Prevot, M. 1977. Variations of the magnetic properties in a basaltic dyke with concentrated cooling zones. Phys. Earth. Planet. Int., 14, pp.120-136.

Tucholke, B., Vogt, P., et al. 1975. Glomar Challenger drills in the North Atlantic. Geotimes, 20, December 1975, pp.18-21.

Zijderveld, J.D.A. 1967. A C demagnetization of rocks: analysis of results. In: Methods in Paleomagnetism. Edited by D.W. Collinson, K.M. Creer, and S.K. Runcorn. Elsevier, Amsterdam, The Netherlands, pp.254-286.

Appendix I Core Description

Graphic Summary

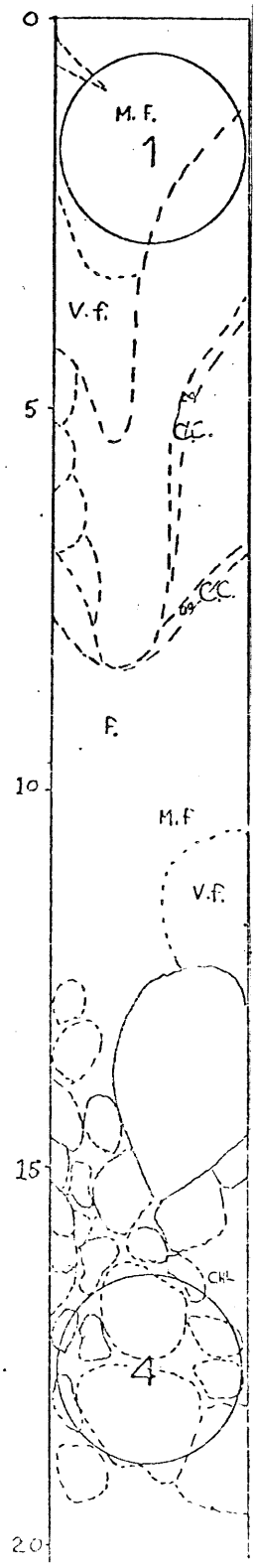

Core Description

Depth: 0 to 8.5 cm. Medium to fine-grained basalt grading to very fine-grained basalt with a sharp contact with the underlying chloritized volcaniclastic breccia. Calcite filled fractures and fine-grained mafic porphyroclasts occur in the breccia.

Depth: 8.5 to 12.5 cm. Fine-grained basalt. Chloritization decreases downward and basalt has fine breccia and calcite inclusions.

Depth: 12.5 to 16 cm. Chloritized breccia margin. Brecciation and chloritization decreases away from the margin to basalt with fine-grained mafic porphyroclasts. Calcite infilling occurs between breccia clasts.

Depth: 16.5 to 20 cm. Angular breccia, calcite, and fine breccia occurs between fine to medium grained basalt clasts. Chloritization occurs in the upper breccia margin.

Graphic Summary

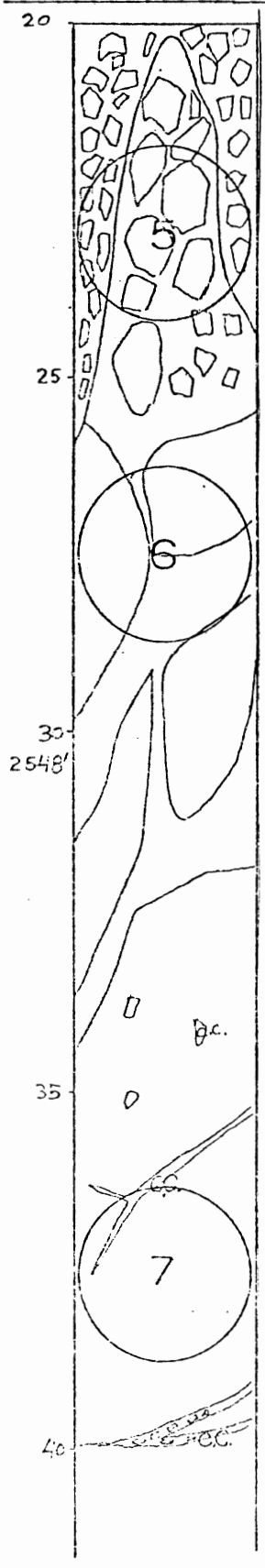

Core Description

Depth: 20 to 26 cm. Unsorted angular breccia clasts in a chloritized calcitic matrix with fine-grained breccia inclusions. Breccia clast size and sorting decreases away from the core axis.

Depth: 26 to 33 cm. 2 cm to 3 cm breccia clasts occur with porphyritic mafic inclusions. Chloritization occurs at base.

Depth: 33 to 43 cm. Fine-grained basalt with calcite filled fractures and fine breccia inclusions.

Graphic Summary

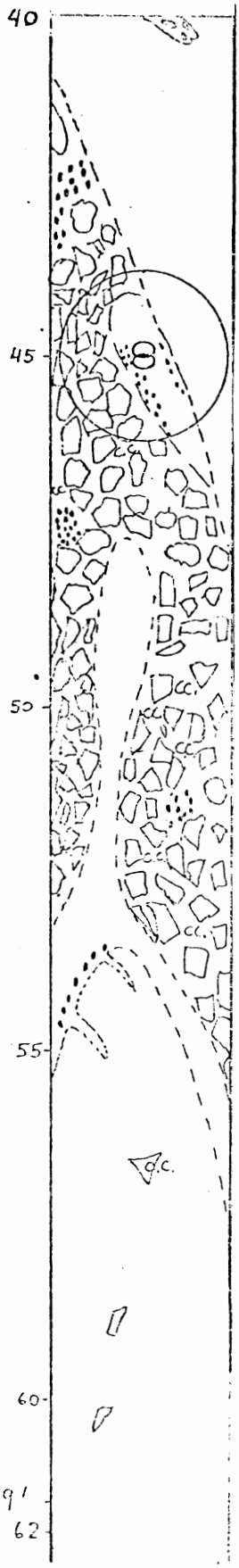

Core Description

Depth: 43 to 54 cm. This core section intersects a sub-vertical pillow margin. Fine sub-angular to round layered breccia with 0.2 to 0.5 cm clasts and abundant mafic porphyroclasts up to 0.5 cm have a vertical lineation trend. Chloritization and calcite porphyrocryst inclusions occur throughout. Reverse side of core consists of fine-grained layered basalt with breccia fracture filling.

Depth: 54 to 60 69 cm. Fine-grained, poorly sorted breccia in a calcitic matrix. The base of the breccia is highly mafic with minor chloritization.

Graphic Summary

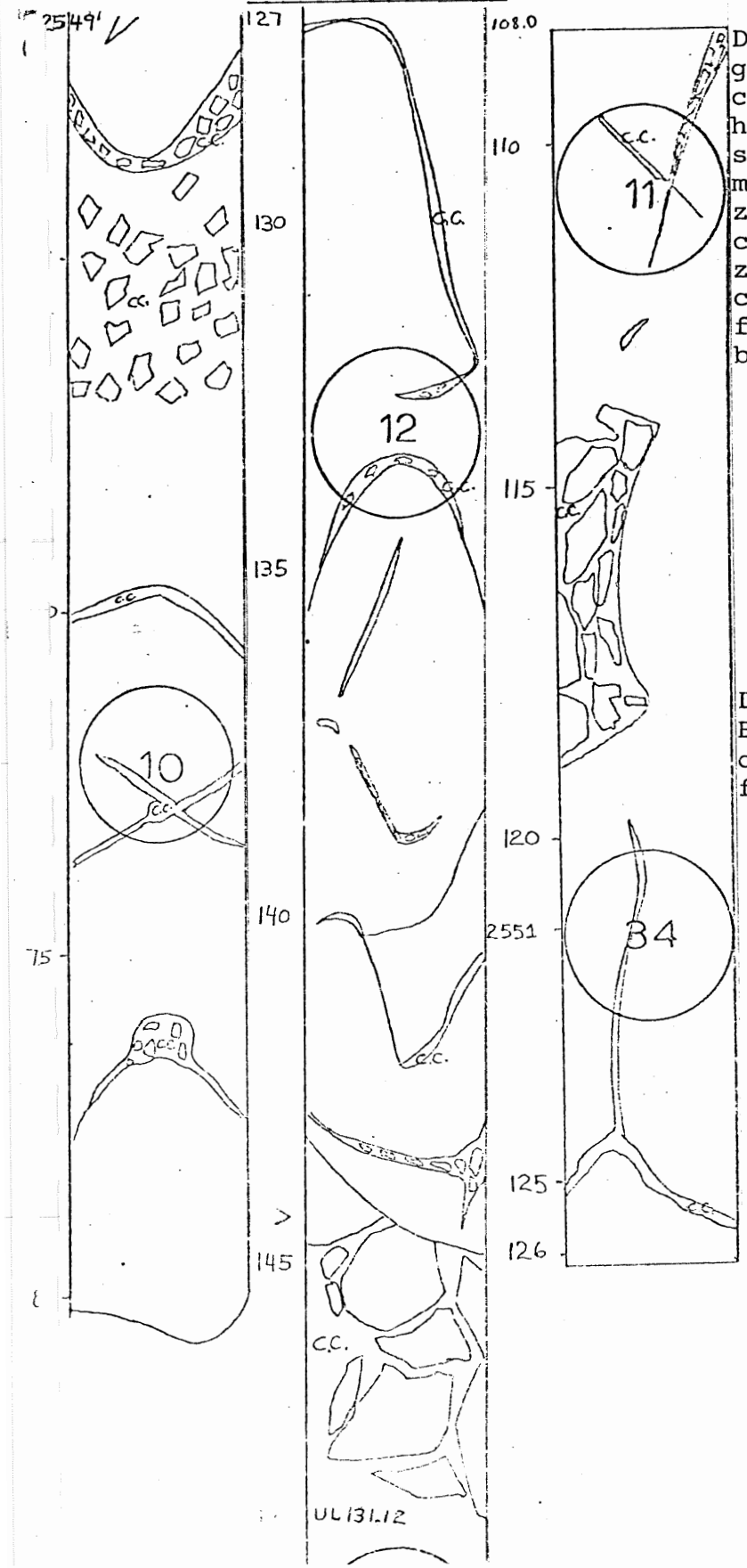

Core Description

Depth: 60 to 144 cm. Fine-grained basalt with numerous calcite filled fractures having fine breccia inclusions and chloritized margins. Basalt and breccia zones have mafic porphyroclasts 134 cm to 143 cm is a zone of frequent interconnected calcite filled fractures and fine-grained breccia.

Depth: 144 to 149 cm. Breccia with 0.25 to 2.0 cm clasts and calcite filled fractures

Graphic Summary

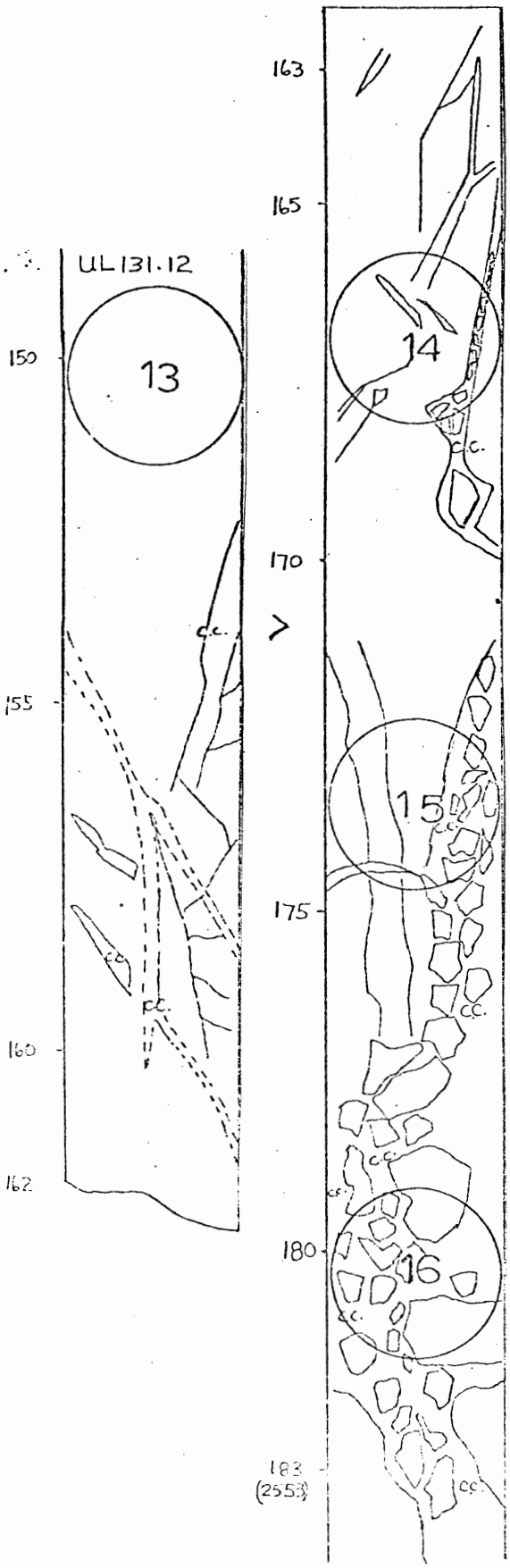

Core Description

Depth: 149 to 162 cm. Fine to medium grained basalt with dendritic calcite veining and breccia inclusions on reverse side of core.

Depth: 162 to 172 cm. Consolidated medium coarse breccia with numerous calcite veins. There is a 1 cm wide calcite breccia zone and transition to fine-gained breccia in a calcitic matrix at the base of the core interval.

Depth: 172 to 188 cm. Breccia with clasts up to 1.5 cm in a calcite filled fractured matrix with minor chlorite alteration. Volume of breccia, calcite and mafic porphyroclasts increases downward over interval.

Graphic Summary

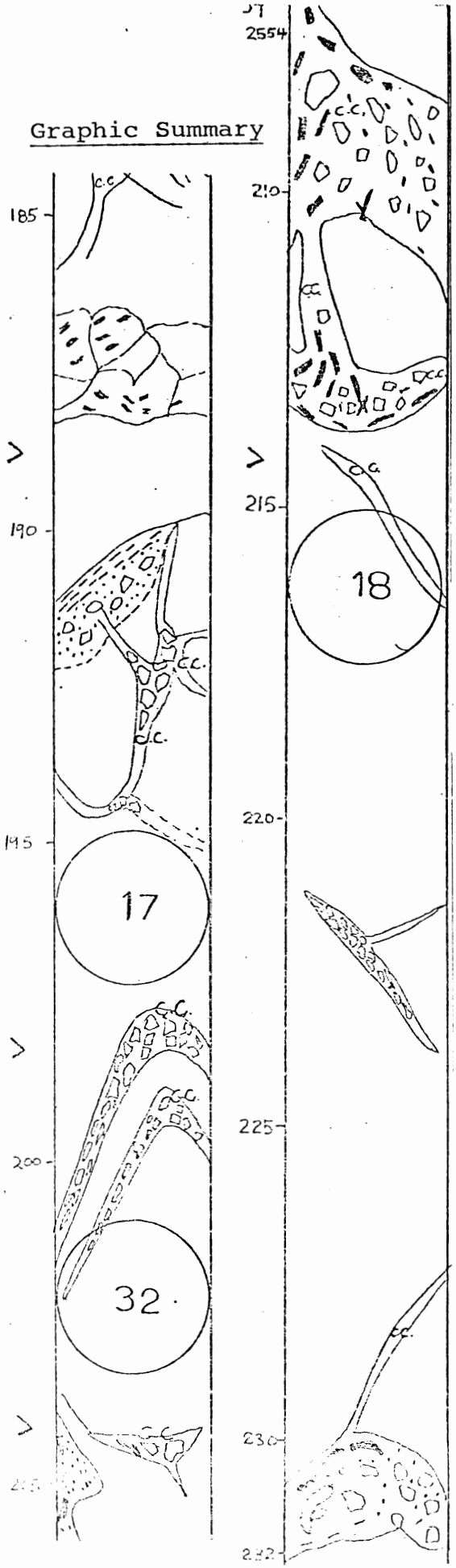

Core Description

Depth: 191 to 193 cm. Zone of chloritized mafic porphyroclasts and minor breccia.

Depth: 193 to 204 cm. Basalt with calcite filled fractures having breccia inclusions.

Depth: 204 to 214 cm. Breccia in a mafic and calcite matrix. Minor chloritization throughout and calcite matrix increases toward base.

Depth: 214 to 230 cm. Medium to fine grained basalt with calcite filled fractures and minor breccia inclusions.

Graphic Summary

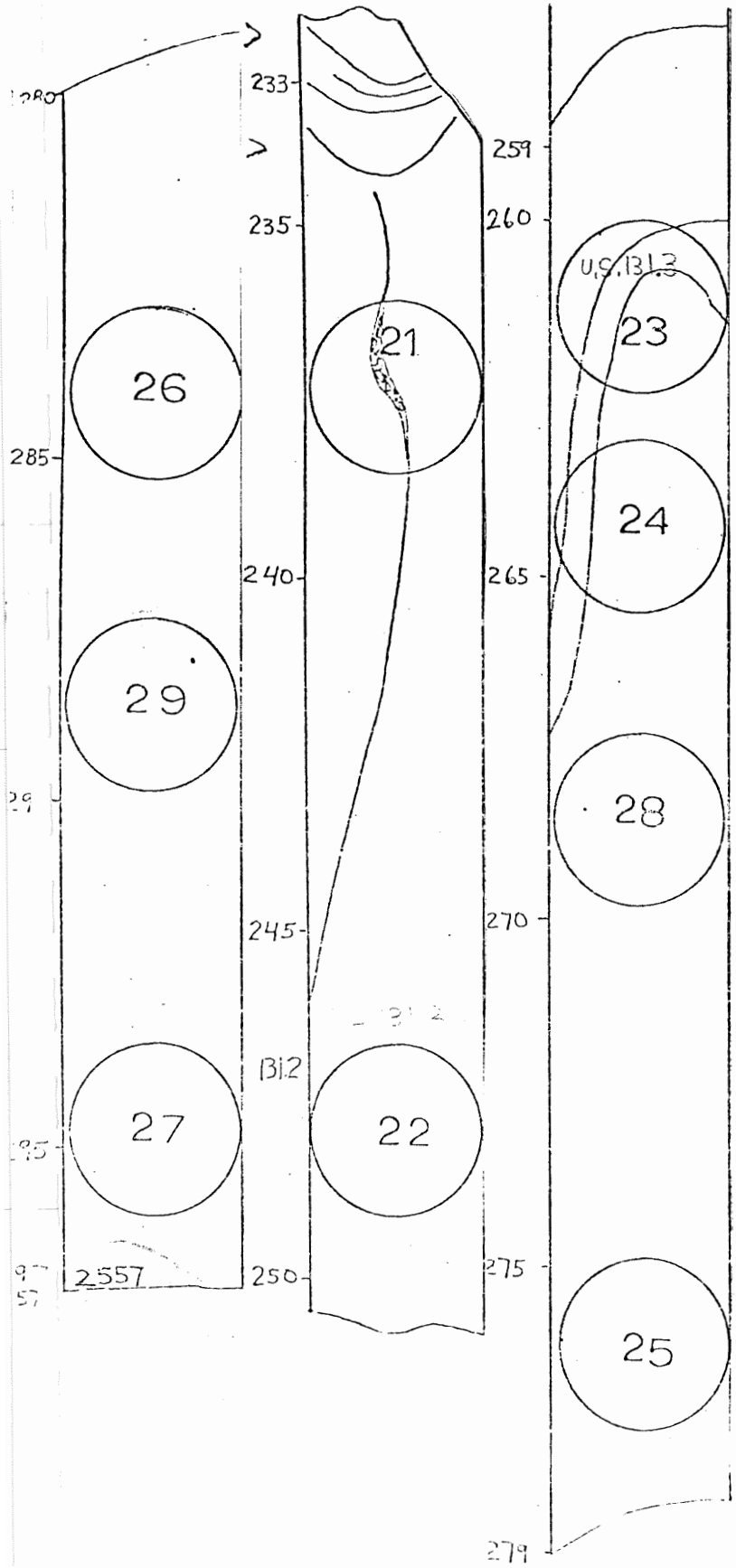

Core Description

Depth: 230 to 232 cm. Gradation from fine-grained basalt to breccia with mafic porphyroclasts.

Depth: 232 to cm. Basalt with grey to dark grey color variation with calcite phenocrysts and pyrit on fracture surfaces.

Depth: 234 to 297 cm. Medium to fine grained basalt with occasional calcite filled fractures and unit sheet 131.3 at 261 cm. Coarse breccia in calcite vein at 286 cm.

Appendix 2. Thin Section Description

SAMPLE 1: Basalt

Texture: Merocrystalline to vitreous groundmass

Groundmass: very fine-grained plagioclase, 1 mm to microlitic plagioclase in a mottled brown vitreous matrix with chlorite alteration.

vitreous matrix:	40%
plagioclase:	35%
calcite:	20%
opaque:	4%
vesicles:	Few, about 2%, quartz and calcite filled.

The opaque minerals are disseminated in the matrix and concentrated along vesicles and fractures. Some opaques have associated hematite staining. Vitreous to microlitic breccia occurs in quartz and calcite filled fractures.

SAMPLE 4: Basalt. fine-grained

Texture: merocrystalline to porphyritic with vitreous matrix

Phenocrysts: subhedral to anhedral plagioclase, 1 mm, finer grained than 1.

Groundmass:

vitreous matrix:	40%, more mottled brown alteration than in 1.
plagioclase:	1 mm, 30%, minor spherulitic plagioclase.
calcite and quartz:	15%, fracture filling and amygdales.
opaque:	3%, concentrated in groundmass and around vesicles and fractures.

vesicles and amygdales: 5% quartz and calcite filled.
alteration: 10% chlorite, highly altered.

SAMPLE 5: Basalt. fine to medium grained

Texture: merocrystalline to a vitreous matrix.

Groundmass: Highly brecciated, very poorly sorted, calcitic and vitrophyric.

groundmass: plagioclase is coarser grained than in Sample 4.
vitreous matrix: 25%
plagioclase: subhedral, very fine grained, 1.5 mm, 35%
calcite and quartz: 30%
opaque: 5%, intersertal in matrix and in mafic pods.
alteration: mottled brown groundmass with 5% chlorite alteration.

SAMPLE 6: Basalt. fine to medium grained

Texture: merocrystalline to insertal matrix, slightly finer grained than Sample 5.

Groundmass: Vitrophyric breccia inclusions of spherulitic plagioclase with insertal plagioclase, 1 mm, in a mottled brown matrix.

plagioclase: 60% intersertal
calcite: 30% fracture filling
opaque: 10% concentrated adjacent to breccia fragments and calcite filled fractures.
alteration: very minor chlorite

SAMPLE 7: Basalt

Texture: vitreous to hyalopilitic

Groundmass: vitreous matrix: 30%
plagioclase: spherulitic to fine-grained (1.5 mm), 40%
Calcite: 25% vein and fracture filling with vitreous plagioclase matrix breccia inclusions.
opaque: 5%, concentrated along calcite filled fractures and vesicles.
vesicles and amygdales: 5%
alteration: minor chlorite

SAMPLE 8: Basalt

Texture: Intersertal plagioclase in a hyalopilitic to vitreous matrix.

Groundmass: Highly mottled brown with numerous spherulites.

plagioclase: 70% 1 mm, finer grained than Sample 7.
opaque: 10%
amygdales and vesicles: 20%, quartz and calcite vein and. fracture filling.
alteration: minor chloritization of quartz quartz and calcite phenocrysts

SAMPLE 10: Basalt

Texture: hyalopilitic

Groundmass: highly altered vitreous matrix

plagioclase: 50%, spherulitic to intersertal, 1 mm, slightly coarser than Sample 8.)
calcite: present in few amygdales and vesicles.
chlorite with clay mineral (montmorillonite void filling.
opaque: 5%, indistinct and disseminated in a highly altered matrix.

alteration: matrix is very highly altered with chlorite, and groundmass is mottled green-brown.

SAMPLE 12: Basalt. medium to fine grained

Texture: intersertal

Groundmass: vitreous matrix: 30%
plagioclase: 40% 1.5 mm
calcite and quartz: 15% vein and fracture filling
opaque: 15% disseminated throughout matrix
vesicles: 2% to 3%
alteration: very minor chlorite

SAMPLE 13: Basalt

Texture: hyalopilitic to intersertal

Phenocrysts: calcite 1.5 to 2.0 mm

Groundmass: variolitic with microlitic to intersertal plagioclase

plagioclase: 60%, 1.5 mm, slightly coarser than Sample 12.
quartz and calcite: 30%, in vesciles, amygdales and veins
opaque: 5%, concentrated in mafic pods.
alteration: very minor chloritization in amygdales and calcite filled fractures.

SAMPLE 14: Basalt. fine to medium grained

Texture: intersertal

Groundmass: variolitic matrix: 15% with consolidated breccia clasts.

plagioclase: 50%, 1.5 mm intersertal with spherulites.
calcite: 20%, amygdale and 1 vein filling.
opaque: 10% disseminated in the groundmass and in pods adjacent to calcite filled fractures.
alteration: 3% minor chlorite

SAMPLE 15: Basalt

Texture: intersertal to hyalopilitic

Phenocrysts: few plagioclase laths 2 mm

Groundmass: variolitic matrix, 30%
plagioclase: 40%, intersertal to spherulitic, 1 mm
quartz and calcite: 20%, amygdale filling.
opaque: 8%, adjacent to calcite filled fractures and disseminated in matrix.
alteration: very minor chloritization, 3%

SAMPLE 16: Basalt

Texture: highly brecciated hyalopilitic to intersertal matrix with minor spherulites.

Phenocrysts: few plagioclase laths 1 mm.

Groundmass: 30%, variolitic matrix
plagioclase: 40%, intersertal to spherulitic 1.5 mm.
calcite: 25%, vesicle and fracture filling.
opaque: 5%, disseminated in matrix and concentrated around vesicle margins.
alteration: very minor chlorite

SAMPLE 17: Basalt. fine-grained

Texture: Spherulitic to holocrystalline with minor pilotaxitic texture.

Phenocrysts: Few plagioclase laths (1.5 mm) and calcite phenocrysts

Groundmass:
- plagioclase: 50%, hyalopilitic plagioclase matrix, 1 mm.
- calcite: 25%, amygdale and vesicle filling.
- opaque: 10%, indistinct in matrix.
- alteration: light to dark brown mottled matrix prevalent with very minor chlorite.

SAMPLE 18: Basalt

Texture: highly altered hyalopilitic with intersertal plag.

Phenocrysts: few plagioclase laths, 1.5 mm.

Groundmass: vitreous, highly chloritized groundmass, 40%.

- plagioclase: 25%, 1.0 mm.
- quartz and calcite: 20%, vein, vesicle and fracture filling with chloritized breccia inclusions.
- opaque: 10% opaque and plagioclase obscure in a chloritized matrix.
- vesicles and amygdales: 5%, quartz, chalcedony and chlorite filled.
- alteration: chlorite prevalent throughout and groundmass highly altered with mottled brown material.

SAMPLE 21: Basalt

Texture: Spherulitic with minor pilotaxtic texture.

Groundmass: variolitic matrix: 20% with epidote
plagioclase: 65%, microlitic to very fine-grained, 1 mm.
opaque: 10%, very fine-grained and disseminated throughout matrix.
vesicles: 5%
alteration: chlorite 7% and mottled brown alteration disseminated throughout matrix.

SAMPLE 22: Basalt. very fine-grained

Texture: granular holocrystalline to intersertal

Phenocrysts: few calcite phenocrysts.

Groundmass: clinopyroxene: 40% anhedral to subhedral, intersertal
plagioclase: 35%, subhedral to euhedral with microlites 1 mm. Slightly coarser than in Sample 21.
calcite: 5% in amygdales and vesicles.
opaque: 10% disseminated throughout matrix, and coarser grained than Sample 21.
alteration: chlorite approximately 7%. This sample has less mottled brown matrix than in Sample 21.

SAMPLE 23: Basalt

Texture: granular holocrystalline to intersertal.

Phenocrysts: few calcite phenocrysts

Groundmass: clinopyroxene: 45% subhedral to anhedral, intersertal.
plagioclase: 40% subhedral to euhedral. Coarser grained than in Sample 22.
calcite: 5%, amygdales and vesicles.
opaque: 10% disseminated throughout matrix. Coarser grained than in Sample 22.
alteration: chlorite alteration around calcite filled amygdales and vesicles.

SAMPLE 24: Basalt

Texture: granular holocrystalline to intersertal, aphyric.

Groundmass: clinopyroxene: 40% subhedral to anhedral in dense microgranular intersertal matrix.
plagioclase: 40% microlitic
opaque: 10%
alteration: chloritization associated with calcite amygdales.
Calcite phenocrysts as pseudomorphs after olivine.

SAMPLE 25: Basalt

Texture: granular holocrystalline to intersertal, aphyric.

Groundmass: clinopyroxene: 30%, with corrosion texture and poikrolitic inclusions.
plagioclase: 35%, equigranular microlites in groundmass.
chlorite: 30%, in amygdales; filled with quartz, calcite and chlorite having granular to isotropic texture.
opaque: 5%, disseminated.

SAMPLE 26: Basalt

Texture: holocrystalline to granular.

Groundmass: plagioclase: 35%, 1.5 mm. Subhedral to euhedral. Possibly sanidine and nepheline.
clinopyroxene: subhedral to anhedral 1.0 to 1.5 mm. Coarser grained than in Sample 25.
opaque: 3%-5%
alteration: brown to green alteration of mafic fraction.
Calcite and chlorite filled vesicles and possible calcite phenocrysts after olivine.

SAMPLE 27: Basalt

Texture: subhedral to anhedral granular with intersertal to variolitic plagioclase.

Phenocrysts: calcite, up to 1.5 mm.

Groundmass: plagioclase: 40%, 1 mm, intersertal to variolitic matrix.
clinopyroxene: 35%, 1 mm anhedral to subhedral.
opaque: 5%
chloritization: disseminated and fracture filling.

Sample 27 is finer grained and less granular than Sample 26.

Appendix 3. Polished Section Description

SAMPLE 1. The groundmass contains disseminated to anhedral 5 u titanomagnetite and titanomaghemite. Anhedral 140 u titanomagnetite porphyroblasts are associated with 15 u to 10 u titanomagnetite grains. Most porphyroclasts are granulated and some have cores of residual unaltered titanomagnetite. .10 u to 4 u dark brown to black highly granulated alteration, which may be partly sphene, occurs throughout the matrix and adjacent to altered porphyroclasts. Hydrothermal alteration state is predominantly M_3 to M_4.

SAMPLE 4. The groundmass contains disseminated subhedral to anhedral 10 u titanomagnetite and titanomaghemite, coarser and more abundant than in Sample 1. Anhedral to subhedral 10 u titanomagnetite grains occur with patchy, grey-white titanomaghemite inclusions in larger grains. Granulated alteration, is less frequent than in Sample 1 and isolated 120 u dark brown granulated alteration zones, possibly relict porphyroclasts, occur within the matrix. Predominant alteration state is L_2 to L_4 with pods of M_3 - M_4 alteration.

SAMPLE 5. The groundmass contains disseminated subhedral to anhedral 10 u titanomagnetite and titanomaghemite in a breccia matrix. Cracking and granulation occurs within some titanomaghemite grains. Titanomagnetite porphyroclasts 50 u to 70 u, have patchy, grey-white titanomaghemite inclusions and are partially granulated. Isolated 5 u to 70 u porphyroclasts of black to dark brown granular alteration (sphene?) occurs. Alteration state is M_2 to M_3.

SAMPLE 6. The groundmass contains disseminated subhedral to anhedral 10 u titanomagnetite and titanomaghemite, slightly finer grained and less abundant than in Sample 5, in a breccia matrix. Few cracked or granulated titanomaghemite grains occur.

Subhedral 10 u titanomaghemite porphyroclasts are present. Subhedral 15 u titanomagnetite porphyroclasts have patchy titanomaghemite inclusions. Granulated alteration, M_3, is less abundant than in 5 and more localized. L_1 to M_1 matrix titanomagnetite alteration predominates with minor M_2-M_3 alteration of titanomaghemite. Minor sulfide occurs as discrete bluish-white grains.

SAMPLE 7. The groundmass contains disseminated subhedral to anhedral 10 u titanomagnetite and titanomaghemite with disseminated sphene. Anhedral to subhedral 10 u titanomagnetite with patchy titanomagnetite inclusions. Localized granular 5 u titanomaghemite occurs. Dark brown to black sphene bearing alteration zones 20 u to 40 u occur. Titanomaghemite and granulated alteration is concentrated rear calcite filled veins. Three size and alteration generations occur: 1) fine-grained titanomagnetite 2) coarse-grained titanomagnetite with titanomaghemite 3) Sphene replacement of black to dark brown granular titanomagnetite alteration. M_2 and M_3 alteration states predominate. Minor sulfide occurs as discrete blue-white and yellow-white grains.

SAMPLE 8. The groundmass contains about 50% dark brown to black granulated alteration with disseminated black sphene. Minor 10 u titanomagnetite and titanomaghemite occurs in the matrix as well as finely disseminated anhedral to subhedral 5 u titanomaghemite. The titanomagnetite, titanomaghemite grains and the granulated alteration zones represent two size generations. The M_3 to M_4 alteration states predominate with minor M_2 alteration. Minor sulfide is present as yellow-white grains.

SAMPLE 10. The groundmass contains two size generations of titanomagnetite within a matrix of abundant dark brown to black granulated alteration up to 40 u. Titanomagnetite occurs as abundant 40 u to 20 u porphyrocrysts and subhedral to anhedral 10 u grains. Porphyrocrysts are cracked and granulated. Smaller

titanomagnetite grains have patchy grey-white titanomaghemite inclusions. Granulated zones represent M_3 to M_4 alteration while small titanomagnetite grains have L_3 to M_2 alteration. Minor sulfide occurs as blue-white grains.

SAMPLE 11. The groundmass contains disseminated subhedral to anhedral 3.5 u to 5 u titanomaghemite and equally abundant 3.5 u to 5 u granulated grains. Subhedral to anhedral 10 u titanomagnetite grains occur with varying degrees of titanomaghemite replacement. Granulation occurs along intra grain cracks and irregular grain boundaries indicating an M_3 alteration state. Granulation of some grains is complete (M_4 alteration).

SAMPLE 12. The groundmass contains disseminated subhedral to anhedral 3.5 u to 5 u titanomaghemite which is less abundant than in 11. Two alteration phases of titanomagnetite occur. There is unaltered dark grey 10 u subhedral to equant titanomagnetite with limited grain boundary cracking. Patchy titanomaghemite replacement alteration also occurs in 10 u titanomagnetite grains. Highly granulated 10 u titanomaghemite phenocrysts occur as well as dark brown to black sphene bearing alteration zones indicating an M_3 to M_4 alteration state. Minor yellow-white to blue-white sulfide grains occur.

SAMPLE 13. The groundmass contains disseminated subhedral to anhedral 3.5 to 5 u titanomaghemite and titanomagnetite. Granulation occurs in 110 u to 40 u titanomaghemite phenocrysts and granulation is complete in some grains, indicating an M_3-M_4 alteration state.

SAMPLE 14. The groundmass contains very minor finely disseminated 4 u subhedral to anhedral titanomagnetite with some grains having skeletal texture. Few subhedral to anhedral 10 u titanomagnetite has irregular and granulated margins suggesting M_2 alteration. Titanomaghemite phenocrysts, 20 u to 360 u,

have M_3-M_4 granulation alteration. Dark brown to black sphene bearing granulated alteration zones up to 40 u occur throughout the groundmass.

SAMPLE 15. The groundmass consists of abundant subhedral to anhedral 3.5 to 5 u granulated titanomagnetite and titanomaghemite. Subhedral 70 to 40 u titanomaghemite porphyroclasts occur with alteration ranging from internal granulation and grain boundary granulation to patchy replacement titanomaghemite-titanomagnetite alteration. Alteration state ranges from L_3 to M_3-M_4.

SAMPLE 16. The groundmass consists of abundant dark brown granulated material in porphyroclasts up to 70 u. Anhedral to subhedral 5 u to 10 u titanomaghemite occurs as remanents of highly altered porphyroclasts, and disseminated throughout the matrix together with altered titanomagnetite. Unaltered titanomagnetite forms a very minor part of the matrix.

SAMPLE 18. The groundmass contains granulated 100 u titanomaghemite porphyroclasts with minor disseminated subhedral to anhedral 10 u titanomaghemite and titanomagnetite with titanomaghemite replacement. Sphene occurs as inclusions in granulated alteration zones up to 40 u in size and finely disseminated black granules.

SAMPLE 21. The groundmass consists of subhedral to anhedral 10 u titanomagnetite, most without alteration to titanomaghemite. Many grains have cracked grain boundaries with minor granulation indicating L_2-L_3 alteration. Curved intragrain cracks have associated granulation alteration. Matrix granulation is very minor.

SAMPLE 22. The groundmass contains subhedral to anhedral 20 u titanomagnetite. Alteration involves patchy titanomaghemite replacement and grain boundary cracking. Minor granulation occurs within grains. Alteration ranges from L_3 to L_4. Subhedral 20 u titanomaghemite grains have well developed cracking and internal granulation. Many titanomaghemite grains are completely granulated and grains are completely fractured, indicating M_3 to M_4 alteration. Matrix alteration is very minor.

SAMPLE 24. Subhedral to anhedral 40 u titanomagnetite grains have well developed internal cracking and most have some alteration to titanomaghemite with granulation. Subhedral 20 u titanomaghemite grains have less granulation associated with grain cracks than titanomagnetite. No phenocrysts occur and matrix granulation is minor. The main oxidation state is M_2-M_3.

SAMPLE 25. Subhedral 15 u to 30 u titanomagnetite is less common than in Sample 24. Titanomagnetite has internal cracking and most have some titanomaghemite inclusions and granulation. Granulation occurs around titanomagnetite grains and fractures. Subhedral to anhedral 20 u to 70 u titanohematite has internal cracking and granulation. Granulated grain aggregates are dark brown to black-brown and up to 100 u. Titanohematite remanents occur within highly granulated titanohematite porphyrocrysts. M_3-M_4 is the major alteration state. Minor yellow-white sulfide grains occur.

SAMPLE 27. Anhedral to subhedral 15 u to 40 u titanohematite is present and some grains show dark brown alteration adjacent to the grain margin and internal granulation. Subhedral 40 u titanomaghemite grains have patchy titanomagnetite inclusions and granulation occurs in most grains. Phenocrysts up to 70 u occur. Groundmass granulation is minor.

Approximate Time Spent on Thesis

core description		30 hours
sample preparation		25 hours
magnetic data collection		40 hours
thin section and polished section description		50 hours
drafting and figure preparation		25 hours
analysis and writing	2 months or	450 hours
	TOTAL	620 hours